

On reduced modelling of the modulational dynamics in magnetohydrodynamics

S. Jin ^{1,2,†} and I.Y. Dodin ^{1,2}

¹Department of Astrophysical Sciences, Princeton University, Princeton, NJ 08543, USA

²Princeton Plasma Physics Laboratory, Princeton, NJ 08540, USA

(Received 20 February 2024; revised 29 August 2024; accepted 25 September 2024)

This paper explores structure formation in two-dimensional magnetohydrodynamic (MHD) turbulence as a modulational instability (MI) of turbulent fluctuations. We focus on the early stages of structure formation and consider simple backgrounds that allow for a tractable model of the MI while retaining the full chain of modulational harmonics. This approach allows us to systematically examine the validity of popular closures such as the quasilinear approximation and other low-order truncations. We find that, although such simple closures can provide quantitatively accurate approximations of the MI growth rates in some regimes, they can fail to capture the modulational dynamics in adjacent regimes even qualitatively, falsely predicting MI when the system is actually stable. We find that this discrepancy is due to the excitation of propagating spectral waves (PSWs) which can ballistically transport energy along the modulational spectrum, unimpeded until dissipative scales, thereby breaking the feedback loops that would otherwise sustain MIs. The PSWs can be self-maintained as global modes with real frequencies and drain energy from the primary structure at a constant rate until the primary structure is depleted. To describe these waves within a reduced model, we propose an approximate spectral closure that captures them and MIs on the same footing. We also find that introducing corrections to ideal MHD, conservative or dissipative, can suppress PSWs and reinstate the accuracy of the quasilinear approximation. In this sense, ideal MHD is a ‘singular’ system that is particularly sensitive to the accuracy of the closure within mean-field models.

Key words: astrophysical plasmas, plasma instabilities, plasma nonlinear phenomena

1. Introduction

1.1. Motivation

Coherent-structure formation from turbulence is ubiquitous in nature, intrinsically compelling and one of the precious few aspects of turbulence that are relatively yielding to analytical efforts (Hussain 1986; Smolyakov, Diamond & Malkov 2000; Krashennikov, D’Ippolito & Myra 2008; Karimabadi *et al.* 2013). For magnetohydrodynamic (MHD) turbulence (Biskamp 2003; Beresnyak 2019; Schekochihin

† Email address for correspondence: sjin@pppl.gov

2022) and the turbulent-dynamo problem (Brandenburg, Sokoloff & Subramanian 2012; Rincon *et al.* 2016; Tobias 2021), this has spawned a vast body of work known as mean-field electrodynamics, or mean-field dynamo theory (Moffatt 1978; Krause & Rädler 1980; Gruzinov & Diamond 1994; Rädler 2007; Brandenburg 2018). In such approaches, the velocity and magnetic fields are split into fluctuations and mean, or average, fields (the definition of average depends on the problem); then, various closures are implemented to obtain the mean-field evolution in response to the fluctuations (Pouquet, Frisch & Léorat 1976; Kraichnan 1977; Nicklaus & Stix 1988; Blackman & Field 2002; Brandenburg & Subramanian 2005*b*).

These closures ultimately rely on a truncation of a formally infinite chain of correlation functions of increasingly high order.¹ This is a common approach to reduced modelling of nonlinear systems, and one can expect it to work when the fluctuations are small compared with the mean field. However, in turbulent structure formation, the usual roles of perturbation and background are switched, that is, mean fields emerge as small modulations of order-one correlation functions that characterize turbulent fluctuations. Hence, the question of the validity of low-order closures becomes non-trivial.

In this paper, we are concerned with the popular closure called the first-order smoothing (Krause & Rädler 1980) or second-order correlation approximation (Rädler 1982). It implies that the mean-field evolution is determined only by second-order correlations of the fluctuations, which, in a broader context, is also known as the quasilinear approximation (Dodin 2022). On the one hand, one can expect its validity domain to be extremely limited. It can be rigorously justified only for small magnetic Reynolds numbers or short correlation times (Brandenburg & Subramanian 2005*a*; Rincon 2019), and comparisons with direct numerical simulations (DNS) often corroborate this expectation (Schrinner *et al.* 2005; Pipin & Proctor 2008). On the other hand, the quasilinear approximation endures in its popularity as a workhorse that is too convenient to cast aside in analytical calculations (Masada & Sano 2014; Squire & Bhattacharjee 2015; Lingam & Bhattacharjee 2016; Gopalakrishnan & Singh 2023). Furthermore, in some cases, quasilinear calculations have been found to produce good agreement with DNS even outside of their formal validity domain (Käpylä *et al.* 2006).² It is therefore important to understand when, and how exactly, the quasilinear approximation fails. Answering this question requires exploring a mean-field model that retains high-order correlations. That is what the present paper is about.

1.2. Outline

Here, we explore structure formation in MHD turbulence as a modulational instability (MI) (Zakharov & Ostrovsky 2009) of the flow-velocity and magnetic-field fluctuations comprising the background turbulence. (For a recent overview of this approach in application to drift-wave and hydrodynamic turbulence, see Tsiolis, Zhou & Dodin (2020) and Zhu & Dodin (2021).) For simplicity, we restrict our consideration to two-dimensional (2-D) turbulence. Although bounded planar flows cannot sustain long-lasting magnetic fields in two dimensions (an antidynamo theorem by Zeldovich (1957)), 2-D turbulence nevertheless hosts rich physics and has long served as a popular testing ground for various aspects of MHD turbulence theory due to its (relative)

¹Here, we use the term ‘truncation’ to refer to low-order closures in general, as opposed to precisely the closure choice of setting all correlations to zero after some cutoff. The latter, which we will refer to as a simple truncation, is done in the quasilinear approximation discussed below but not, for example, in the various τ approximations (Brandenburg & Subramanian 2005*b*; Blackman & Field 2002).

²Confusingly, various analytical closures and DNS can conflict and agree in various combinations (Zhou & Blackman 2021); but this issue is beyond the scope of the present paper.

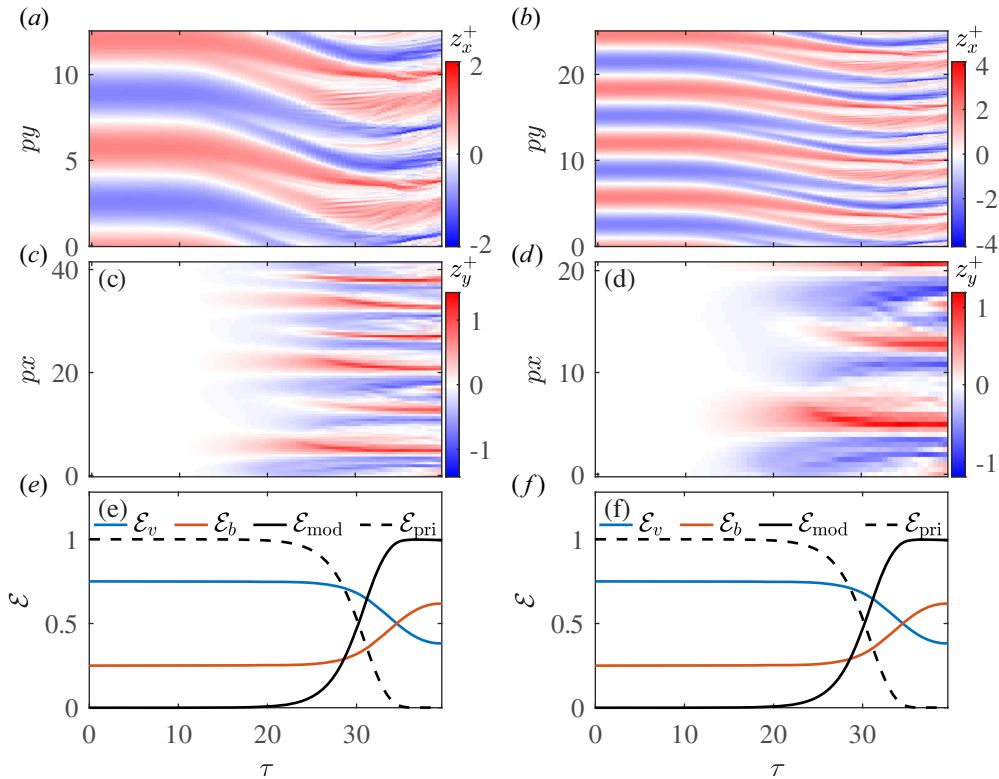


FIGURE 1. The DNS of modulational dynamics of (2.3) seeded at $\tau = 0$ with random noise. (This figure is discussed in detail in later sections. For the notation, see §§ 2.1 and 2.2.) Panels (a,c,e) correspond to a modulationally unstable primary mode (2.17) with $\theta^\pm = \pm\pi/6$, and (b,d,f) correspond to a modulationally stable primary mode with $\theta^\pm = \pm\pi/3$. Panels (a,b) show $z_x^+(t, y)$, (c,d) show $z_y^+(t, x)$ and (e,f) show the corresponding energy breakdown. Specifically, \mathcal{E}_v is the normalized kinetic energy (2.21c), $\mathcal{E}_b = E_b/E_{\text{tot}}$ is the normalized magnetic energy (2.21d), \mathcal{E}_{mod} is the normalized modulational-mode energy (2.21b) and \mathcal{E}_{pri} is the normalized primary-mode energy (2.21a). The colour bar shows the field amplitudes normalized to \mathcal{A}/p . The spatial coordinates are normalized to $1/p$.

tractability (Pouquet 1978; Biskamp, Schwarz & Drake 1996; Biskamp & Schwarz 2001; Nazarenko 2007; Giorgio, Servidio & Veltri 2017). The goal of this paper is to complement those works with a detailed study of MIs using both reduced models and DNS.

Specifically, we study how energy is transferred from primary fluctuations to mean magnetic field and mean velocity during the early stages of structure formation, when these mean fields are weak and the primary structure can be treated as fixed. To analyse this process in detail, we assume a maximally reduced model of the turbulent fluctuations, namely, a spatially monochromatic primary structure. The simplicity of this model has been detracting attention from it in the literature in favour of more realistic turbulence settings, but there is more to it that meets the eye. Even with a monochromatic primary structure, the modulational dynamics remains remarkably intricate and, depending on the system parameters, can change drastically (figure 1) in ways that are not captured by the common closures or obvious from the standard eigenmode analysis (Friedberg 1987). However, the simplicity of our model helps unravel this mystery.

We find that, when the primary structure truly experiences a MI, this MI can be described well with typical truncated models that neglect high-order correlations. However, already in adjacent regimes, such truncated models can fail spectacularly and produce false positives for instability. To study this process in detail, we propose an ‘extended’ quasilinear theory (XQLT) that treats the primary structure as fixed but includes the entire spectrum of modulational harmonics (as opposed to just the low-order harmonics, as usual). From XQLT, also corroborated by DNS, we find that the difference between said regimes is due to a fundamental difference in the structure of the modulational spectrum. For unstable modes, the spectrum is exponentially localized at low harmonic numbers, so truncated models are justified. But this localization does not always occur. At other parameters, modulational modes turn into constant-amplitude waves propagating down the spectrum, unimpeded until dissipative scales. These spectral waves are self-maintained as global modes with real frequencies and cause ballistic energy transport along the spectrum, breaking the feedback loops that could otherwise sustain MI. The ballistic transport drains energy from the primary structure at a constant rate until the primary structure is depleted. Notably, these effects are overlooked if one assumes from the start that the modulation spectrum is confined and that, accordingly, dissipation entirely vanishes in the limit of zero viscosity and resistivity.

A comment is due here regarding how the established truncated MHD closures fit into this picture. Given the indispensability of such simple closures, a higher-resolution understanding of their limitations can help guide and interpret their inevitable application. For example, we show that both conservative and dissipative corrections to ideal MHD tend to restore the validity of the quasilinear approximation. In this sense, ideal incompressible MHD is a ‘singular’ theory that is particularly sensitive to the accuracy of the closure within mean-field models. That said, it is an important conclusion of our work that, unless deviations from ideal incompressible MHD are substantial, changing the turbulence parameters even slightly can produce qualitative inaccuracies in an otherwise workable reduced model. Therefore, efforts to extrapolate closures or infer them from general considerations should be supplemented with first-principle calculations based on the underlying modulational dynamics. As a step in this direction, we propose a spectral closure that captures both the propagating spectral waves (PSWs) and MIs within our model. (But, of course, more work remains to be done for generic MHD turbulence.)

The paper is organized as follows. In § 2, we present the basic equations and derive the XQLT. In § 3, we examine the ability of truncated models of low-order to predict the MI rate. In § 4, we introduce spectral waves and describe their properties. In § 5, we propose a closure that can simultaneously capture MIs and spectral waves. In § 6, we demonstrate the impact of corrections to ideal MHD on the modulational dynamics. In § 7, we summarize our main results. Auxiliary calculations are presented in appendices.

2. Extended quasilinear theory

2.1. Base model

2.1.1. Incompressible resistive MHD

As a base model, we assume incompressible resistive MHD with homogeneous mass density $\rho = \text{const}$. The corresponding governing equations are

$$\partial_t \mathbf{v} + (\mathbf{v} \cdot \nabla) \mathbf{v} = (\mathbf{b} \cdot \nabla) \mathbf{b} - \nabla P + \nu \nabla^2 \mathbf{v}, \quad (2.1a)$$

$$\partial_t \mathbf{b} = \nabla \times (\mathbf{v} \times \mathbf{b}) + \eta \nabla^2 \mathbf{b}. \quad (2.1b)$$

Here \mathbf{v} is the fluid velocity; $\mathbf{b} \doteq \mathbf{B}/\sqrt{4\pi\rho}$ is the local Alfvén velocity (the symbol \doteq denotes definitions), i.e. rescaled magnetic field \mathbf{B} ; $P \doteq (P_{\text{kin}} + B^2/8\pi)/\rho$ is the

normalized total pressure, with P_{kin} being the kinetic pressure. Also, ν is the viscosity and η is the resistivity, both of which are assumed either constant or negligible (except at small enough scales). Due to incompressibility and magnetic Gauss's law, one also has

$$\nabla \cdot \mathbf{v} = 0, \quad \nabla \cdot \mathbf{b} = 0. \tag{2.1c}$$

In order to put (2.1) in a more symmetric form, let us rewrite them in terms of the two Elsässer fields \mathbf{z}^\pm (Elsässer 1950), which are also solenoidal,

$$\mathbf{z}^\pm \doteq \mathbf{v} \pm \mathbf{b}, \quad \nabla \cdot \mathbf{z}^\pm = 0. \tag{2.2a,b}$$

This leads to two coupled equations for \mathbf{z}^\pm ,

$$\partial_t \mathbf{z}^\pm = -(\mathbf{z}^\mp \cdot \nabla) \mathbf{z}^\pm - \nabla P + \nu_+ \nabla^2 \mathbf{z}^\pm + \nu_- \nabla^2 \mathbf{z}^\mp, \tag{2.3}$$

where $\nu_+ \doteq (\nu + \eta)/2$ and $\nu_- \doteq (\nu - \eta)/2$. The normalized total pressure P can be found as follows. By taking the divergence of (2.1a) and using (2.2a,b), one obtains

$$\nabla^2 P = -\nabla \cdot [(\mathbf{z}^\mp \cdot \nabla) \mathbf{z}^\pm]. \tag{2.4}$$

Let us introduce the wavevector operator $\hat{\mathbf{k}} \doteq -i\nabla$, so $\hat{k}^2 \doteq \hat{\mathbf{k}}^2 = -\nabla^2$. Let us also assume some appropriate (say, periodic) boundary conditions. Then, (2.4) yields

$$P = -\hat{k}^{-2} \hat{\mathbf{k}} \cdot [(\mathbf{z}^\mp \cdot \hat{\mathbf{k}}) \mathbf{z}^\pm] + \text{const.}, \tag{2.5}$$

whence ∇P in (2.3) can be expressed through \mathbf{z}^\pm . Alternatively, ∇P can be eliminated from (2.3) by taking the curl of this equation and rewriting the result in terms of the Elsässer vorticities

$$\mathbf{w}^\pm \doteq \nabla \times \mathbf{z}^\pm. \tag{2.6}$$

Indeed, due to (2.2a,b), one can express \mathbf{z}^\pm using a vector potential \mathbf{a}^\pm such that $\mathbf{z}^\pm = \nabla \times \mathbf{a}^\pm$. Let us assume the gauge such that $\nabla \cdot \mathbf{a}^\pm = 0$. Then,

$$\mathbf{w}^\pm = \nabla \times (\nabla \times \mathbf{a}^\pm) = -\nabla^2 \mathbf{a}^\pm \equiv \hat{k}^2 \mathbf{a}^\pm, \tag{2.7}$$

whence

$$\mathbf{z}^\pm = i\hat{k}^{-2} (\hat{\mathbf{k}} \times \mathbf{w}^\pm). \tag{2.8}$$

(Here, we assume that \mathbf{z}^\pm have zero spatial average, so \hat{k}^2 is invertible.) Then, (2.3) can be expressed through \mathbf{w}^\pm alone,

$$\partial_t \mathbf{w}^\pm = -\hat{\mathbf{k}} \times \{[(\hat{\mathbf{k}} \times \hat{k}^{-2} \mathbf{w}^\mp) \cdot \hat{\mathbf{k}}] (\hat{\mathbf{k}} \times \hat{k}^{-2} \mathbf{w}^\pm)\} - \hat{k}^2 (\nu_+ \mathbf{w}^\pm + \nu_- \mathbf{w}^\mp). \tag{2.9}$$

2.1.2. The 2-D collisionless model

For simplicity, below we adopt a 2-D model, meaning that \mathbf{z}^\pm lie in the (x, y) plane and $\partial_z = 0$. In this case, the only potentially non-zero component of \mathbf{w}^\pm is the z -component, $w^\pm \doteq (\nabla \times \mathbf{z}^\pm)_z$. We also forgo an explicit treatment of the viscosities ν_\pm below. (However small, though, these viscosities remain non-negligible in that they determine absorbing boundary conditions at infinity in the spectral space; see § 4.) Then, the vector equation (2.9) can be replaced with a scalar equation for w^\pm ,

$$\partial_t w^\pm = \epsilon_{lmz} \left[\left(\frac{\hat{k}_m}{\hat{k}^2} w^\mp \right) (\hat{k}_l w^\pm) - \left(\frac{\hat{k}_n \hat{k}_l}{\hat{k}^2} w^\mp \right) \left(\frac{\hat{k}_n \hat{k}_m}{\hat{k}^2} w^\pm \right) \right], \tag{2.10}$$

where ϵ_{lmz} is the Levi-Civita symbol with the third index fixed to z . Note that the right-hand side of (2.10) vanishes whenever w^+ or w^- is zero. This means that any stationary w^+ is a solution as long as w^- is zero and *vice versa*.

2.1.3. *Fourier representation*

Assuming the Fourier representation

$$w^\pm = \sum_k w_k^\pm(t) \exp(i\mathbf{k} \cdot \mathbf{x}), \tag{2.11}$$

where $\mathbf{x} \doteq (x, y)$, one arrives at the following equation for the Fourier coefficients w_k^\pm :

$$\partial_t w_k^\pm = \sum_{k_1, k_2} T(\mathbf{k}_1, \mathbf{k}_2) w_{k_1}^\mp w_{k_2}^\pm \delta_{\mathbf{k}, \mathbf{k}_2 + \mathbf{k}_1}, \tag{2.12}$$

where the dot is the time derivative, δ is the Kronecker delta, $T(\mathbf{k}_1, \mathbf{k}_2)$ are the coupling coefficients given by

$$T(\mathbf{k}_1, \mathbf{k}_2) = [\mathbf{e}_z \cdot (\mathbf{k}_2 \times \mathbf{k}_1)] \frac{(\mathbf{k}_2 + \mathbf{k}_1) \cdot \mathbf{k}_2}{k_1^2 k_2^2}, \tag{2.13}$$

and \mathbf{e}_j is the unit vector along the j th axis. Accordingly, the kinetic and magnetic energy are given by

$$E_v = \frac{\rho}{8} \sum_k \frac{1}{k^2} |w_k^+ + w_k^-|^2 \equiv \sum_k E_{v,k}, \tag{2.14a}$$

$$E_b = \frac{\rho}{8} \sum_k \frac{1}{k^2} |w_k^+ - w_k^-|^2 \equiv \sum_k E_{b,k}, \tag{2.14b}$$

where $E_{v,k}$, and $E_{b,k}$ are the corresponding spectral energy densities. Then, the total energy density is

$$E = \frac{\rho}{4} \sum_k \frac{1}{k^2} (|w_k^+|^2 + |w_k^-|^2) \equiv \sum_k E_k, \tag{2.15}$$

where E_k is the spectral total-energy density.

2.2. *Harmonic coupling mediated by a primary structure*

2.2.1. *Equation for the modulational spectrum*

Let us explore modulational stability of a Fourier harmonic with a given wavevector $\mathbf{k} = \mathbf{p}$ and the corresponding order-one Fourier amplitudes w_p^\pm . We will call it the primary harmonic or, primary structure. Let us choose axes such that $\mathbf{p} = p\mathbf{e}_y$, and assume a perturbation with a wavevector \mathbf{q} . As can be seen from (2.13), non-trivial coupling requires a component of \mathbf{q} perpendicular to \mathbf{p} , and the component of \mathbf{q} parallel to \mathbf{p} does not qualitatively affect the modulational dynamics.³ For simplicity then, let us assume $\mathbf{q} = q\mathbf{e}_x$. Let us also assume initial conditions such that at $t = 0$, $w_p^\pm = O(1)$, and $w_{q+np}^\pm = O(\epsilon)$, where $\epsilon \ll 1$ is a small parameter.⁴ (Remember that $O(\epsilon)$ means, loosely speaking, ‘scales as ϵ or smaller’ but not necessarily ‘of order ϵ ’.) This ordering is not guaranteed to hold as the system evolves (for example, a MI corresponds to exponential growth of w_{q+np}^\pm), but it will hold at least for some initial linear stage; i.e. equations resulting from this ordering will describe the linear growth of a MI but not its saturation.

³As shown below, the modulational dynamics is determined mostly by the asymptotic form of the coefficients α_n^\pm and β_n^\pm (introduced in § 2.2.2) at large n , and this form is insensitive to the component of \mathbf{q} parallel to \mathbf{p} .

⁴Multiple, incommensurate q s may also be present, as the modulational dynamics along each corresponding slice of wavenumbers $\mathbf{k} = \mathbf{q} + n\mathbf{p}$ evolve independently.

For early times such that primary mode remains dominant, the largest contributions to the sum in (2.12) have $k_1 = p$ or $k_2 = p$. To first order in ϵ we then have

$$\begin{aligned} \partial_t w_k^\pm &\approx T(p, k_-) w_p^\mp w_{k_-}^\pm + T(-p, k_+) w_{-p}^\mp w_{k_+}^\pm \\ &+ T(k_-, p) w_{k_-}^\mp w_p^\pm + T(k_+, -p) w_{k_+}^\mp w_{-p}^\pm, \end{aligned} \tag{2.16}$$

where $k_\pm \doteq k \pm p$ and $k = q + np$ with integer n . (All the five terms in (2.16) are of order ϵ , so, whether or not one chooses to introduce ϵ explicitly in this equation, the small parameter cancels out in any case. For the same reason, (2.16) is invariant with respect to rescaling $w_k^\pm \rightarrow C w_k^\pm$, where C is any non-zero constant.) For all other k , one obtains $\partial_t w_k^\pm = O(\epsilon^2)$ and therefore negligible within the assumed approximation. In particular, this means that w_p^\pm can be considered fixed; i.e. $A^\pm \doteq w_p^\pm \approx \text{const}$. In terms of the Elsässer fields, this corresponds to a primary structure

$$z^\pm = -\frac{2}{p} \mathcal{A}^\pm \sin(py + \theta^\pm) \mathbf{e}_x, \tag{2.17}$$

where $\mathcal{A}^\pm \doteq |A^\pm|$ and $\theta^\pm \doteq \arg A^\pm$.

For the modulation energy density and the primary-wave energy density,

$$E_{\text{mod}} \doteq \sum_{k=q+np} E_k = \sum_n \frac{\rho}{4} \sum_{\sigma=\pm 1} \frac{|w_{q+np}^\sigma|^2}{q^2 + n^2 p^2}, \tag{2.18a}$$

$$E_{\text{pri}} \doteq E_p = \frac{\rho}{4} \sum_{\sigma=\pm 1} \frac{|w_p^\sigma|^2}{p^2}, \tag{2.18b}$$

one has

$$\frac{dE_{\text{mod}}}{dt} = \sum_n \frac{\rho}{4} \sum_{\sigma=\pm 1} \frac{w_{q+np}^{\sigma*} \partial_t w_{q+np}^\sigma}{q^2 + n^2 p^2} + \text{c.c.}, \tag{2.19a}$$

$$\frac{dE_{\text{pri}}}{dt} = \frac{\rho}{4} \sum_{\sigma=\pm 1} \frac{w_p^{\sigma*} \dot{w}_p^\sigma}{p^2} + \text{c.c.}, \tag{2.19b}$$

where ‘c.c.’ stands for ‘complex conjugate’. Using

$$\partial_t w_p^\sigma = \sum_{k=q+np} T(k, p - k) w_k^{-\sigma} w_{p-k}^\sigma, \tag{2.20}$$

for $k = q + np$, one finds that our approximate equations conserve the total energy density $E_{\text{tot}} = E_{\text{pri}} + E_{\text{mod}}$ exactly within this approximation. (For brevity, from now on we will refer to the energy densities simply as energies.) We will assume that the initial modulational energy is negligible, so $E_{\text{tot}} = \rho \mathcal{A}^2 / 4p^2$, where $\mathcal{A}^2 \doteq (\mathcal{A}^+)^2 + (\mathcal{A}^-)^2$, and we will also use the following dimensionless energies:

$$\mathcal{E}_{\text{pri}} = E_{\text{pri}} / E_{\text{tot}}, \tag{2.21a}$$

$$\mathcal{E}_{\text{mod}} = E_{\text{mod}} / E_{\text{tot}}, \tag{2.21b}$$

$$\mathcal{E}_v = E_v / E_{\text{tot}}, \tag{2.21c}$$

$$\mathcal{E}_b = E_b / E_{\text{tot}}. \tag{2.21d}$$

2.2.2. Dimensionless equations

In order to reduce the number of free parameters, let us perform a variable transformation $w_{q+np}^\pm \mapsto \psi_n^\pm$,

$$w_{q+np}^\pm = \sqrt{\frac{\mathcal{A}^3(q^2 + n^2p^2)}{\mathcal{A}^\mp p^2}} \exp\left(in\frac{\theta^+ + \theta^-}{2}\right) \psi_n^\pm, \tag{2.22}$$

where $\psi_n^\pm = O(\epsilon)$. Then, (2.16) becomes

$$\begin{aligned} \partial_t \psi_n^\pm &= \mathcal{A}^\mp e^{\mp i\theta} \alpha_n^\mp \psi_{n-1}^\pm + \sqrt{\mathcal{A}^+ \mathcal{A}^-} e^{\pm i\theta} \beta_n^\mp \psi_{n-1}^\mp \\ &+ \mathcal{A}^\mp e^{\pm i\theta} \alpha_n^\pm \psi_{n+1}^\pm + \sqrt{\mathcal{A}^+ \mathcal{A}^-} e^{\mp i\theta} \beta_n^\pm \psi_{n+1}^\mp, \end{aligned} \tag{2.23}$$

where $\theta \doteq (\theta^+ - \theta^-)/2$ and α_n^\pm and β_n^\pm are given by

$$\alpha_n^\pm \doteq \mp r \frac{r^2 + n(n \pm 1)}{\sqrt{(r^2 + n^2)(r^2 + (n \pm 1)^2)}}, \tag{2.24a}$$

$$\beta_n^\pm \doteq -r \frac{n}{\sqrt{(r^2 + n^2)(r^2 + (n \pm 1)^2)}}. \tag{2.24b}$$

Note that these coefficients depend only on the ratio $r \doteq q/p$ rather than on q and p separately. From (2.23), one can also see that the phases θ^+ and θ^- *per se* are, expectedly, unimportant and the dynamics is affected by these phases only in the combination $\theta^+ - \theta^-$.

It is also convenient for our purposes to introduce

$$\tau \doteq \mathcal{A}t \tag{2.25}$$

as the new dimensionless time, as well as $\phi \doteq \arctan(\mathcal{A}^-/\mathcal{A}^+) \in [0, \pi/2]$, so that

$$\mathcal{A}^+ = \mathcal{A} \cos \phi, \quad \mathcal{A}^- = \mathcal{A} \sin \phi. \tag{2.26a,b}$$

In particular, $\phi = 0$ and $\phi = \pi/2$ correspond to structures consisting only of w_p^+ and w_p^- , respectively, and $\phi = \pi/4$ corresponds to a ‘balanced’ background with $\mathcal{A}^+ = \mathcal{A}^-$. For simplicity, $\phi = \pi/4$ will be assumed from now on throughout the paper (except where specified otherwise). In this case (for $\phi = \pi/4$), one has

$$\frac{E_{\text{pri},b}}{E_{\text{pri},v}} = \frac{|w_p^+ - w_p^-|^2}{|w_p^+ + w_p^-|^2} = \tan^2 \theta, \tag{2.27}$$

where $E_{\text{pri},v}$ and $E_{\text{pri},b}$ are the kinetic and magnetic energy densities in the primary mode, respectively. Hence, θ can be understood as the parameter that determines the relative weights of the kinetic and magnetic-field energy in the primary-mode energy. In particular, $\theta = 0$ corresponds to a primary structure that involves only velocity perturbations, while $\theta = \pi/2$ corresponds to a primary structure that involves only magnetic-field perturbations.

Using this notation, one can express (2.23) in the following compact form:

$$\dot{\psi}_n = \sum_{\sigma=\pm 1} G_n^\sigma \psi_{n+\sigma} \tag{2.28}$$

(the dot denotes ∂_τ), or even more compactly as

$$\dot{\psi} = M\psi. \tag{2.29}$$

Here, $\psi_n \doteq (\psi_n^-, \psi_n^+)^\top$ is a two-component column vector (the symbol \top denotes transposition), $\psi \doteq (\dots, \psi_{-1}, \psi_0, \psi_1, \dots)^\top$ is an infinite-dimensional block vector consisting of ψ_n , the matrices G_n^σ are given by

$$G_n^\sigma \doteq \begin{pmatrix} \alpha_n^\sigma \cos \phi \exp(-i\sigma\theta) & \beta_n^\sigma \sqrt{\cos \phi \sin \phi} e^{i\sigma\theta} \\ \beta_n^\sigma \sqrt{\cos \phi \sin \phi} \exp(-i\sigma\theta) & \alpha_n^\sigma \sin \phi e^{i\sigma\theta} \end{pmatrix} \tag{2.30}$$

and M is the following block matrix:

$$M \doteq \begin{pmatrix} \ddots & & & \vdots & & & \ddots \\ & 0 & G_{-2}^+ & 0 & 0 & 0 & \\ & G_{-1}^- & 0 & G_{-1}^+ & 0 & 0 & \\ \dots & 0 & G_0^- & 0 & G_0^+ & 0 & \dots \\ & 0 & 0 & G_1^- & 0 & G_1^+ & \\ & 0 & 0 & 0 & G_2^- & 0 & \\ \ddots & & & \vdots & & & \ddots \end{pmatrix}. \tag{2.31}$$

It is readily seen then that the system’s dynamics is controlled only by the dimensionless parameters r, θ and ϕ , while \mathcal{A} and p determine only its characteristic temporal and spatial scales, respectively.

The dimensionless modulational energy (2.21b), or

$$\mathcal{E}_{\text{mod}} \doteq \sum_{\sigma} \frac{\mathcal{A}}{\mathcal{A}^{-\sigma}} |\psi_n^\sigma|^2 \equiv \sum_n \mathcal{E}_n, \tag{2.32}$$

is governed by

$$\dot{\mathcal{E}}_n = \sum_{\sigma} (I_n^\sigma + F_n^\sigma) + \text{c.c.}, \tag{2.33}$$

where I_n and F_n are given by

$$I_n^\sigma = \frac{\mathcal{A}\sqrt{\mathcal{A}^\sigma}}{(\mathcal{A}^{-\sigma})^{3/2}} (\beta_n^- e^{i\sigma\theta} \psi_{n-1}^{-\sigma} + \beta_n^+ \exp(-i\sigma\theta) \psi_{n+1}^{-\sigma}) \psi_n^{\sigma*}, \tag{2.34}$$

$$F_n^\sigma = \frac{\mathcal{A}}{\mathcal{A}^{-\sigma}} (\alpha_n^- \exp(-i\sigma\theta) \psi_{n-1}^\sigma + \alpha_n^+ e^{i\sigma\theta} \psi_{n+1}^\sigma) \psi_n^{\sigma*}. \tag{2.35}$$

Because $\sum_n F_n^\sigma = 0$, the terms F_n^σ represent the energy flux that is carried along the modulation spectrum and is conserved within each subchannel σ . In contrast, I_n can be

understood as injection terms in that they also appear, with the opposite signs, in the equation for the primary wave,

$$\dot{\mathcal{E}}_{\text{pri}} = - \sum_n \sum_{\sigma=\pm 1} I_n^\sigma + \text{c.c.}, \tag{2.36}$$

which follows from (2.20). Note that the energy in each subchannel σ is separately conserved, i.e. both energy and cross-helicity are conserved.

Equations (2.28) and (2.29) are similar to the equations that describe a one-dimensional chain of coupled linear oscillators. The n th elementary cell of the chain consists of two different oscillators characterized by ψ_n^+ and ψ_n^- , respectively. Similar equations emerge in studies of phase-space turbulence for the coupling between Hermite moments of the particle phase-space probability distribution (Hammett *et al.* 1993; Kanekar *et al.* 2015; Parker 2016; Adkins & Schekochihin 2018; Nastac *et al.* 2023). Throughout this work, we use (2.28) and (2.29) to study the nature of collective oscillations in the chain of modulational harmonics, which can be understood as Floquet modes of the linearized system. Unstable oscillations of this system (i.e. MIs) lead to structure formation on top of the primary structure.

One can also consider (2.29) as a Schrödinger equation with a Hamiltonian $i\mathbf{M}$. This Hamiltonian is not Hermitian, because modulations are parametrically coupled with the primary mode (through which energy can be either gained or lost) and dissipate at $n \rightarrow \infty$. At the same time, this Hamiltonian is invariant under the time-reversal transformation ($i \rightarrow -i$) and the parity transformation in the spectral space ($n \rightarrow -n, \sigma \rightarrow -\sigma$). This makes the system (2.28) \mathcal{PT} -symmetric (Bender 2005; Bender *et al.* 2019). Depending on the balance of sources and sinks, such systems can support modes with entirely real frequencies (unbroken \mathcal{PT} symmetry) and pairs of modes whose frequencies are mutually complex-conjugate (broken \mathcal{PT} symmetry). This will be discussed further in § 4.

As long as the underlying ordering assumption [$|w_{q+np}^\pm|/|w_p^\pm| \sim O(\epsilon)$] holds, XQLT (2.28) provides an excellent approximation of the modulational dynamics of (2.3) (figure 2). However, practical applications of XQLT require truncations of this system. In the remainder of this work, we discuss to what extent such truncations can be adequate and compare our analytical results with XQLS (numerical simulations of (2.28) with the spectral boundary sufficiently far such that it is never reached in the time simulated), *in lieu* of the full (2.3).

3. Truncated models

3.1. Basic equations

A common way to truncate a problem like (2.29) is to postulate that all ψ_n with $|n| > N$ are negligible. One can also understand this as imposing reflective boundary conditions in the oscillator chain $\{\psi_n^\sigma\}$,

$$\psi_{N+1}^\sigma = \psi_{-(N+1)}^\sigma = 0. \tag{3.1}$$

Retained in this case are harmonics with wavevectors \mathbf{p} and $\mathbf{q} + n\mathbf{p}$, with $n = 0, \pm 1, \dots, \pm N$. This means that the resulting system has $Q = 1 + (1 + 2N)$ degrees of freedom. We call this procedure Q -mode truncation (QMT). The corresponding truncation of ψ will be denoted as ψ_{QMT} , and the corresponding truncation of \mathbf{M} will be denoted as \mathbf{M}_{QMT} , so (2.29) becomes

$$\dot{\psi}_{QMT} = \mathbf{M}_{QMT} \psi_{QMT}. \tag{3.2}$$

Because of (3.1), eigenmodes of this system can be understood as standing waves in the oscillator chain $\{\psi_n^\sigma\}$ and have the form $\psi_{QMT} = Y \exp(-i\omega\tau)$, where ω are global

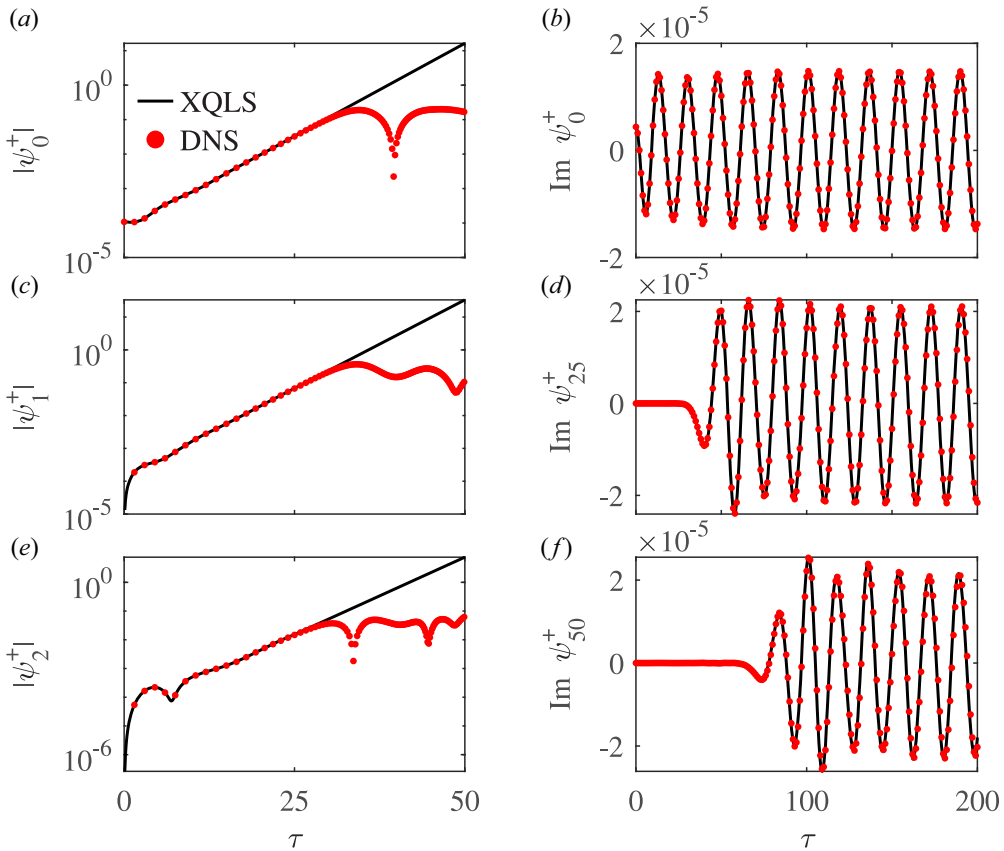


FIGURE 2. Comparison of the time evolution of various ψ_n^+ as predicted by DNS of (2.3) (red dots) and XQLS (numerical simulations of XQLT) (2.28) (black curves) for two representative cases of (a,c,e) the MI ($\theta = \pi/6$) and (b,d,f) stable modulational dynamics ($\theta = \pi/3$). Nonlinear DNS are seeded with random noise, resulting in a broadband modulational dynamics, but the results shown are for a modulation corresponding to $r = 0.5$, and the XQLS are initialized accordingly. For the $\theta = \pi/6$ case, the harmonics shown are (a) $n = 0$, (b) $n = 1$ and (c) $n = 2$. In this case, XQLT adequately approximates the nonlinear dynamics until approximately $\tau \sim 30$. For the $\theta = \pi/3$ case, the harmonics shown are (d) $n = 0$, (e) $n = 25$ and (f) $n = 50$. In this case, XQLT adequately approximates the nonlinear dynamics indefinitely.

frequencies and Y are constant ‘polarization vectors’. According to (2.29), these vectors satisfy $DY = 0$, where $D = i\omega\mathcal{K} + M_{QMT}$ and \mathcal{K} is a unit $Q \times Q$ matrix. Then, ω can be found from

$$\det D = 0 \tag{3.3}$$

and MIs correspond to modes with $\text{Im } \omega > 0$.

The success of this approach hinges on the assumption that higher harmonics truly remain negligible. In other words, a QMT should be able to adequately describe the evolution of a modulational mode if its eigenvector ψ_{QMT} is heavily weighted towards the low-order harmonics. Below, we explore to what extent this assumption is satisfied in various regimes.

3.2. *Growth rates*

The lowest-order QMT is 4MT, which corresponds to $N = 1$. Within this model, the primary harmonic with $\mathbf{k} = \mathbf{p}$ is assumed to interact with the modulational mode at $\mathbf{k} = \mathbf{q}$ only through two sidebands $\mathbf{k} = \mathbf{q} \pm \mathbf{p}$; then, $\boldsymbol{\psi}_{4\text{MT}} = (\boldsymbol{\psi}_{-1}, \boldsymbol{\psi}_0, \boldsymbol{\psi}_1)^\top$ and

$$\mathbf{M}_{4\text{MT}} = \begin{pmatrix} 0 & \mathbf{G}_{-1}^+ & 0 \\ \mathbf{G}_0^- & 0 & \mathbf{G}_0^+ \\ 0 & \mathbf{G}_1^- & 0 \end{pmatrix}. \tag{3.4}$$

(This model can be understood as quasilinear, because, although the modulational dynamics remains nonlinear, the second- and higher-order harmonics of the perturbation are neglected.) The 4MT equations yield

$$\omega^2 = \frac{r^4}{1+r^2} (1 \pm \sqrt{1 - (1 - r^{-4} \cos^2 2\theta) \sin^2 2\phi}). \tag{3.5}$$

(Note that these are normalized frequencies corresponding to the normalized time τ . To obtain the actual physical frequencies, one must multiply the right-hand side of (3.5) by \mathcal{A} .) Assuming $\phi = \pi/4$, one finds that two out of four branches of this dispersion relation are unstable at $|r| < 1$. The corresponding growth rate $\Gamma \doteq \text{Im } \omega$ is maximized at $\theta = 0$ and $\theta = \pi/2$ at the value

$$\Gamma = r \sqrt{\frac{1-r^2}{1+r^2}} \tag{3.6}$$

(from now on, we assume $r > 0$ for clarity of notation), and the corresponding polarization vectors are as follows:

$$\mathbf{Y}_0 = \begin{cases} (1, +1)^\top, & \theta = 0, \\ (1, -1)^\top, & \theta = \pi/2. \end{cases} \tag{3.7}$$

The case $\theta = 0$ can be recognized as a purely hydrodynamic Kelvin–Helmholtz instability, i.e. one that does not involve magnetic field. The case $0 < \theta < \pi/4$ can be understood as the MHD generalization of the Kelvin–Helmholtz instability. Note that the case $\theta = \pi/2$ has the form of the tearing instability (Boldyrev & Loureiro 2018) (and similarly we may understand $\pi/4 < \theta < \pi/2$ as generalizations with shear flow), although the tearing instability should be stable in the ideal limit. However, the stability problem that we are studying here is somewhat different from the stability problem of tearing eigenmodes in that we also address transient dynamics, as will become clearer in § 4.

Potentially more accurate is a model with $N = 2$, or 6MT, which accounts for harmonics with $\mathbf{k} = \mathbf{q} \pm 2\mathbf{p}$; then, $\boldsymbol{\psi}_{6\text{MT}} = (\boldsymbol{\psi}_{-2}, \boldsymbol{\psi}_{-1}, \boldsymbol{\psi}_0, \boldsymbol{\psi}_1, \boldsymbol{\psi}_2)^\top$ and

$$\mathbf{M}_{6\text{MT}} = \begin{pmatrix} 0 & \mathbf{G}_{-2}^+ & 0 & 0 & 0 \\ \mathbf{G}_{-1}^- & 0 & \mathbf{G}_{-1}^+ & 0 & 0 \\ 0 & \mathbf{G}_0^- & 0 & \mathbf{G}_0^+ & 0 \\ 0 & 0 & \mathbf{G}_1^- & 0 & \mathbf{G}_1^+ \\ 0 & 0 & 0 & \mathbf{G}_2^- & 0 \end{pmatrix}. \tag{3.8}$$

One can derive an analytical expression for ω from here just like we derived (3.5) from (3.4). However, this expression is cumbersome and not particularly instructive, so it is not presented explicitly. Truncations with larger Q , albeit also explored by us, will not be presented either for the same reason.

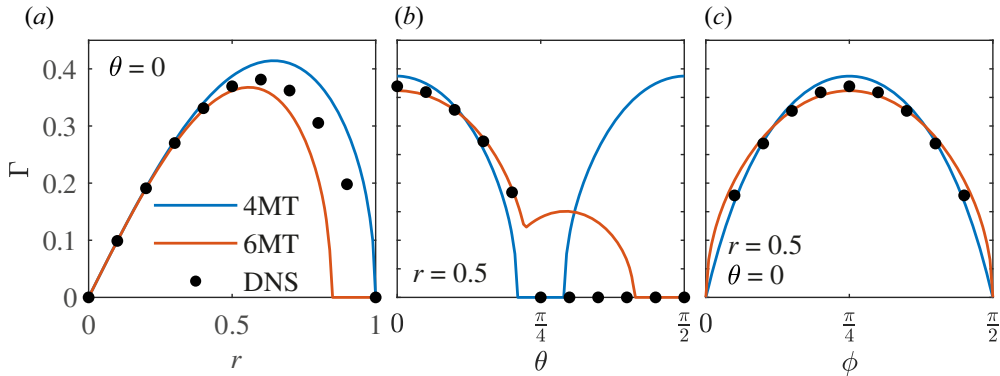


FIGURE 3. (a) The growth rate Γ (of the most unstable mode) versus the normalized wavenumber r at $\theta = 0$: 4MT (blue); 6MT (red); XQLS (black markers). (b) The same for Γ versus θ at $r = 0.5$. The 4MT predicts identical growth rates at $\theta = 0$ and $\theta = \pi$, while the 6MT and XQLS predict that the system is unstable at $\theta = 0$ and stable at $\theta = \pi$. (c) The same for Γ versus ϕ at $r = 0.5$ and $\theta = 0$.

Figure 3 shows a comparison of the 4MT and 6MT predictions and the MI growth rates inferred numerically from XQLS. Note that the truncated models quantitatively agree with each other and with XQLS at some parameters but drastically disagree at other parameters. In particular, the 4MT predicts that Γ is an even function of $\pi/2 - \theta$, while the 6MT predicts that this is not the case. Furthermore, XQLT predicts that, for example, at $r = 0.5$, the system is stable at all $\theta > \pi/2$ (figure 3b). Let us discuss this in detail.

As expected from the analytical formula (3.6) based on the 4MT, and as we have also found numerically, MI is typically suppressed at $r \gtrsim 1$; hence, below we focus on the regime $r \in (0, 1)$. A comparison of the growth rate predicted by XQLT and truncated models in this range is presented figure 4. The corresponding primary modes with $\theta \lesssim \pi/4$ are modulationally unstable, and the growth rates predicted by 4MT and 6MT are in good agreement with XQLT. Such primary structures are dominated by the velocity field, $\mathcal{E}_{\text{pri},v} > \mathcal{E}_{\text{pri},b}$ (see (2.27)), and thus will be called *v*-dominated primary modes (VDPMs). At $\theta \gtrsim \pi/4$, primary structures are dominated by the magnetic field, $\mathcal{E}_{\text{pri},b} > \mathcal{E}_{\text{pri},v}$, and thus will be called *b*-dominated primary modes (BDPMs). As seen in figure 4, BDPMs are modulationally stable, but truncated models predict otherwise. Figure 4(a,b) shows the discrepancy between the predictions of XQLT, 4MT and 6MT for representative parameters, specifically, $\theta \in (0, \pi/2)$ and $\phi = \pi/4$. (Stability is primarily determined by θ and r . Deviations of ϕ from $\pi/4$ result only in quantitative adjustments, unless ϕ is close to 0 or $\pi/2$.) In other words, truncated modes tend to overestimate the growth rate and systematically produce false positives for instability. Figure 5 shows that, although the magnitude of disagreement decreases with N , the systematic overprediction of instability persists.

This can be understood as follows. Consider two possible scenarios for modulational stability. The first possibility is that there is no tendency for the primary mode to inject energy into such a modulation in the first place. (Injection is localized to small $|n|$, so this corresponds to regimes where both low-order QMTs and XQLT predict stability.) Alternatively, the primary mode tends to inject energy but the energy escapes to higher harmonics instead of entering positive feedback loops at low $|n|$. (This corresponds to the false positive case where QMTs predict instability when the system is actually modulationally stable.) This overprediction can therefore be understood as a consequence

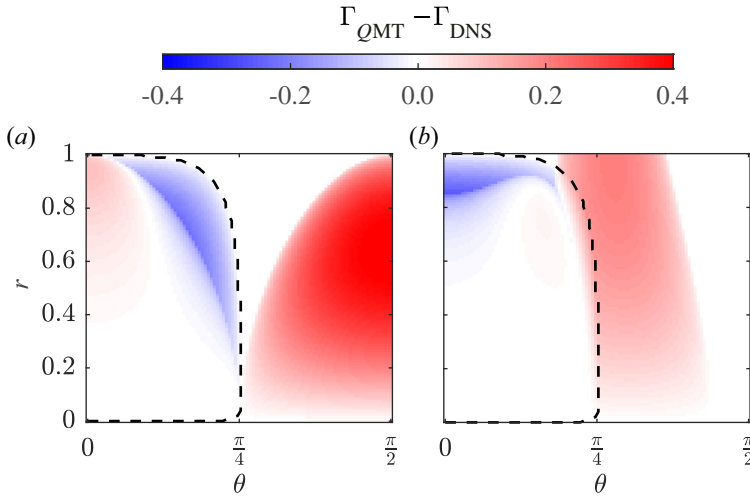


FIGURE 4. The difference between the growth rate predicted by a QMT and that inferred from XQLS, $\Gamma_{QMT} - \Gamma_{XQLS}$, versus (θ, r) for $\phi = \pi/4$: (a) 4MT; (b) 6MT. The dashed curves mark the stability boundary as determined by a parameter scan with XQLS. The preponderance of the red colour, especially outside the instability domain, indicates that truncated models tend to produce false positives for instability.

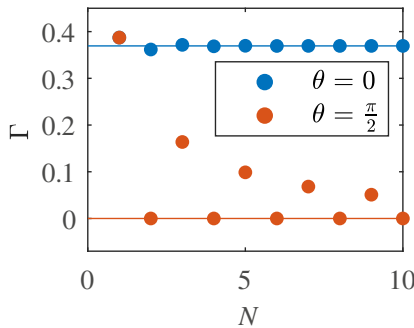


FIGURE 5. The growth rates Γ obtained through a QMT for $\theta = 0$ (blue markers) and $\theta = \pi/2$ (orange markers) versus the number of modes retained, N . The solid-coloured lines indicate the corresponding XQLS growth rates, to which the rates predicted by the truncated models converge at large N .

of simple truncations constituting perfectly reflecting boundary conditions for the energy⁵, i.e. the outward energy flux at the cutoff harmonic $n = N$ is enforced to be zero if $|\psi_{N+1}^{\pm}|$ are held to be zero (2.35). By trapping energy that might otherwise escape to higher $|n|$ at lower harmonics, $QMTs$ can generate false positive feedback loops with injection (2.34). True MIs then correspond to modulational dynamics that naturally remain confined to small $|n|$.

This can be seen by analysing the eigenmode structure. (See also Appendix A for an alternative explanation.) As to be discussed in § 4, unstable modes are evanescent spectral

⁵In contrast, we find through XQLS that $QMTs$ do not conserve anastrophy (i.e. the magnetic potential squared) at the spectral boundary.

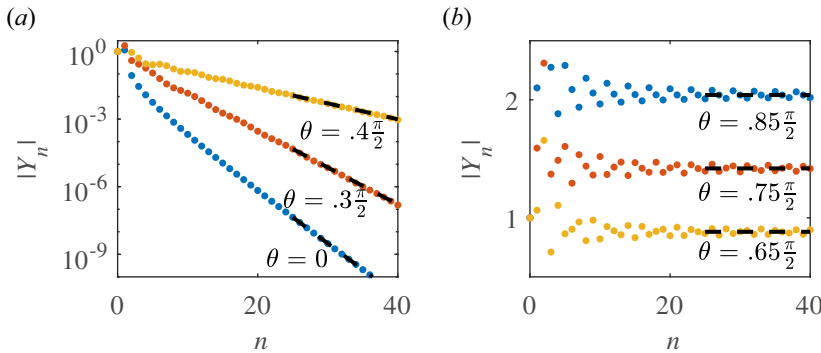


FIGURE 6. Typical structures of eigenmodes, specifically, $|Y_n|$ versus n , at $r = 0.5$ and $\phi = \pi/4$ for various θ : (a) unstable modes supported by VDPMs; (b) oscillatory solutions supported by BDPMs. (The upper index in $|Y_n^\sigma|$ is omitted because $|Y_n^+| = |Y_n^-|$ for the assumed parameters.) Here $|Y_n|$ decreases exponentially with n for the former (notice the logarithmic scale) but asymptote to non-zero constants for the latter. The asymptotes are indicated by the dotted lines. These results are obtained through XQLS using the initial conditions of the form (4.6) and normalized such that $|Y_0| = 1$.

waves, whose $|Y_n|$ exponentially decrease with $|n|$ (figure 6a),

$$|Y_n| \propto \exp(-|n|/l). \tag{3.9}$$

(We assume $\phi = \pi/4$ for simplicity, so $|Y_n^+| = |Y_n^-|$ and the upper index in $|Y_n^\sigma|$ can be omitted.) That is why truncated models correctly predict MI for modes that are actually unstable. The spectral scale l depends on the system parameters, and the smaller l the more accurate QMT is. At some parameters, though, particularly when $\theta \rightarrow \pi/4$, l becomes large or even infinite, such that $|Y_n|$ asymptotes to a non-zero constant at $|n| \rightarrow \infty$ (figure 6b). In this case, QMT is bound to fail. The corresponding modes are PSWs. While they also receive energy from the primary structure at low n , PSWs transport this energy along the spectrum to $|n| \rightarrow \infty$. There, the energy is unavoidably dissipated by viscosity or resistivity, however small those are. Below, we discuss these effects in more detail.

4. Spectral waves

4.1. Dynamics at large $|n|$

First, let us consider spectral waves at $|n| \gg 1$. In this limit, one has $\alpha_n^\pm \rightarrow \mp r$ and $\beta_n^\pm \rightarrow 0$, so (2.29) yields two decoupled wave equations for ψ_n^+ and ψ_n^- ,

$$\dot{\psi}_n^- = r \cos \phi (e^{i\theta} \psi_{n-1}^- - e^{-i\theta} \psi_{n+1}^-), \tag{4.1a}$$

$$\dot{\psi}_n^+ = r \sin \phi (e^{-i\theta} \psi_{n-1}^+ - e^{i\theta} \psi_{n+1}^+). \tag{4.1b}$$

These equations allow solutions in the form of monochromatic waves,

$$\psi_n^\sigma = \Psi^\sigma \exp(-i\omega\tau + iK^\sigma n), \tag{4.2}$$

with constant amplitude Ψ^σ , frequency ω and ‘wavenumber’ K^σ . The quotation marks are added as a reminder that the corresponding waves propagate in the spectral space rather than in the physical space. Also note that K^\pm are defined unambiguously only within the first Brillouin zone, $K^\pm \in (-\pi, \pi)$.

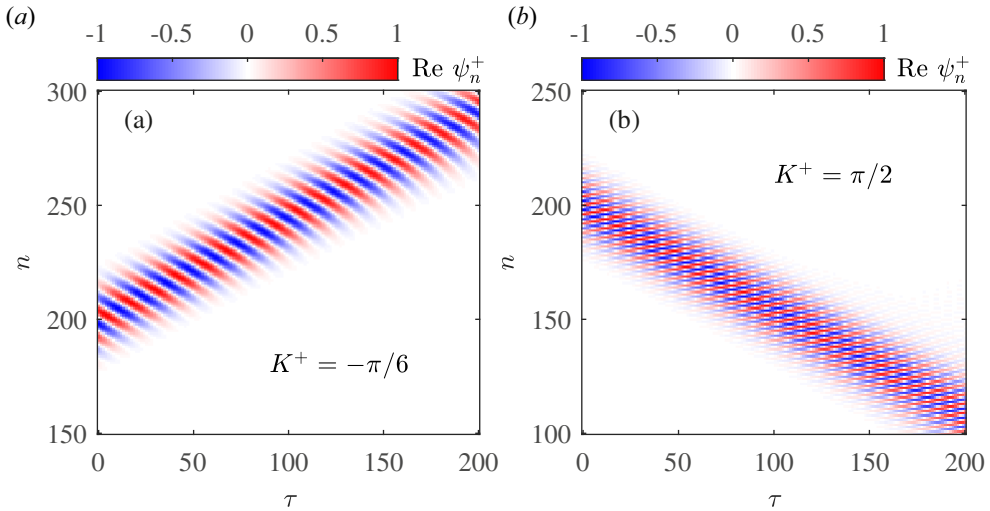


FIGURE 7. Numerical simulations showing PSW packets propagating (a) down the spectrum ($|n|$ of the packet centre increases with time) and (b) up the spectrum ($|n|$ of the packet centre decreases with time). In both cases, $r = 0.5$ and $\theta = \pi/3$. Both packets are initialized using $\psi_n^+(\tau = 0) = \exp[-(n - n_0)^2/\zeta + iK^+n]$ with $n_0 = 200$, $\zeta = 150$, and (a) $K^+ = -\pi/6$, (b) $K^+ = \pi/2$.

From (4.1), one readily finds that spectral waves obey the following dispersion relations:

$$\omega = \omega_0^\sigma \sin \kappa^\sigma, \quad \kappa^\pm \doteq K^\pm \pm \theta, \tag{4.3a,b}$$

where $\omega_0^+ = 2r \sin \phi$ and $\omega_0^- = 2r \cos \phi$. Accordingly, spectral waves in the n space along the ψ^σ channel have the group velocity

$$v_g^\sigma = \omega_0^\sigma \cos \kappa^\sigma \tag{4.4}$$

and can propagate either up or down the spectrum (figure 7). The dependence of ω and v_g^\pm on θ can be removed by a gauge transformation. Specifically, κ^\pm becomes the true wavenumber if one adopts the variables $\bar{\psi}_n^\pm \doteq \psi_n^\pm \exp(\mp i n \theta)$ instead of ψ_n^\pm . Also notably, to the extent that the (large) index n can be approximately considered a continuous variable, (4.1) can be written as usual non-dispersive-wave equations for $\zeta^\pm(\tau, n) \doteq \bar{\psi}_n^\pm(\tau)$,

$$\partial_\tau \zeta^\pm = -\omega_0^\pm \partial_n \zeta^\pm. \tag{4.5}$$

This model corresponds to the small- κ^σ limit of (4.3a,b), that is, $\omega \approx \omega_0^\sigma \kappa^\sigma$.

The above equations can be used to describe PSW packets localized at large $|n|$ but not the global eigenmodes (because the latter involve dynamics at small $|n|$). In particular, (4.3a,b) are not enough to find the global-mode frequencies. Yet they allow one to determine the mode structure at $|n| \gg 1$ if one knows the mode frequency from other considerations (or, *vice versa*, to find the mode frequency if κ^\pm are known). In particular, unstable modes have complex ω , so, according to (4.3a,b), their asymptotic wavenumber cannot be real. This explains why unstable modes are evanescent. In contrast, for real ω , (4.3a,b) allows for real wavenumbers (provided that $|\omega| \leq \omega_0^\pm$), i.e. predicts PSWs. These results are corroborated by XQLS. For example, figure 6 shows the mode structures

inferred from the asymptotic dynamics of $\psi_n^\sigma(\tau)$ at large enough τ for the initial conditions

$$\psi_n^\sigma(\tau = 0) = \begin{cases} \epsilon \exp(i\xi_n^\sigma), & n = \pm 1, \\ 0, & n \neq \pm 1. \end{cases} \quad (4.6)$$

Here, ϵ is a constant small amplitude⁶, and ξ_n are parameters that change the polarization of the initial conditions while keeping the initial modulation energy fixed. (The specific values of ξ_n^σ are given in the captions of figures in which initial condition dependent results of XQLS are presented.) This form of the initial conditions is chosen to emulate a simple modulation of the primary mode.

The fact that the properties of spectral waves are determined only by the asymptotic properties of α_n^\pm and β_n^\pm makes these waves particularly robust. In particular, note that the asymptotic form of α_n^\pm and β_n^\pm at $|n| \rightarrow \infty$ remains the same even when \mathbf{p} and \mathbf{q} are not orthogonal, so the above results readily extend to general \mathbf{q} . Likewise, a similar picture holds also for three-dimensional interactions, although the mode polarization can be more complicated in this case. Notably, PSWs provide ballistic rather than diffusive (or superdiffusive) energy transport along the spectrum. This distinguishes them from the cascades that are commonly discussed in turbulence theories and result from eddy–eddy interactions, or wave–wave collisions (Galtier *et al.* 2000).

4.2. Global modes in the form of PSWs

In realistic settings, spectral waves are excited at finite $|n|$ and propagate down the spectrum. Evanescent waves reach $|n| \sim l$ (see (3.9)) in finite time τ_0 , get reflected, and eventually (asymptotically) settle as stationary standing waves on time scales of the order of a few τ_0 . Such waves can be adequately described by truncated models. In contrast, PSWs continue to propagate towards infinity indefinitely (until they dissipate at scales where viscosity or resistivity is no longer negligible). Thus, they never develop components propagating up the spectrum at large $|n|$ and so they never become quite like the standing-wave eigenmodes predicted by truncated models (§ 3.1). This means that actual PSWs cannot be adequately described by analysing QMT in principle. Instead, they should be considered in the context of the initial-value problem, much like Langmuir waves appear in plasma kinetic theory within Landau’s initial-value approach as opposed to the Case–van Kampen true-eigenmode approach (Stix 1992).

Consequently, even though (2.29) has infinitely many degrees of freedom, the number of relevant global modes, i.e. those that propagate towards infinity, is finite. We find that there are only two of them, which can be attributed to the fact that $\dim \psi_n = 2$. (Likewise, at a given wavenumber, only one, Langmuir, branch of relevant electrostatic waves in electron plasma remains relevant after transients are gone.) For example, for $\phi = \pi/4$, we find from XQLS that

$$\omega = \pm \sqrt{2}r \cos \theta. \quad (4.7)$$

This dependence and the corresponding mode structures are illustrated in figure 8. Each of the two modes has two wavenumbers associated with it: one determines ψ_n^σ at $n \rightarrow +\infty$, and the other one determines $\psi_n^{-\sigma}$ at $n \rightarrow -\infty$ (figure 9). Thus, there are four κ_d^σ overall, where σ denotes the corresponding component of ψ_n , and d denotes the direction

⁶The specific value of ϵ does not matter for the linear dynamics of ψ_n^\pm but can affect how long the linear approximation holds as a result of the evolving linear dynamics. Energy in the modulational channel may grow at the expense of the primary mode, eventually causing the linear approximation to break down. Therefore, throughout the paper when properties involving energy are reported the explicit scaling with ϵ is retained.

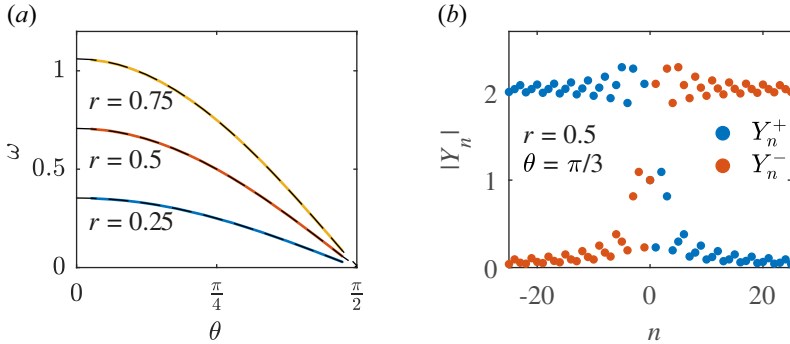


FIGURE 8. (a) The dependence of the global-mode frequency $\omega > 0$ on θ for various r . The dashed lines are the inferred solutions (4.7). (b) Here $|Y_n^+|$ (blue) and $|Y_n^-|$ (orange) for the mode with $\omega > 0$. The eigenmode amplitudes for the $\omega < 0$ mode are identical with the roles of $|Y_n^+|$ and $|Y_n^-|$ switched.

of propagation ($d = \pm 1$ is the sign of the group velocity at $|n| \rightarrow \infty$). They can be found by combining (4.7) with (4.3a,b) and applying $\text{sgn } v_g = d$, i.e. $\omega_0^d \cos \kappa_d^\sigma > 0$. This yields

$$\omega > 0 : \quad \kappa_+^+ = \frac{\pi}{2} - \theta, \quad \kappa_-^- = -\frac{3\pi}{2} + \theta, \quad (4.8a)$$

$$\omega < 0 : \quad \kappa_-^+ = \frac{3\pi}{2} - \theta, \quad \kappa_+^- = -\frac{\pi}{2} + \theta, \quad (4.8b)$$

where $\kappa_d^\sigma = K_d^\sigma + \sigma\theta$ and the values of K_d^σ are defined modulo the Brillouin zone (i.e. $K_-^- = -3\pi/2$ should be understood as $\pi/2$ and so on). Remember, though, that this applies only to global eigenmodes. Transient waves propagating in the region $|n| \gg 1$ can have any κ^σ (figure 7).

The fact that the frequencies of these modes are real indicates that the modes are self-sustained notwithstanding the dissipation that they unavoidably experience at $|n| \rightarrow \infty$. The corresponding evolution of the wave spectrum is illustrated in figure 9(a) and the corresponding evolution in the physical space is shown in figure 10. This remarkable dynamics is understood from the fact that the energy drain via this dissipation is balanced by the energy injection from the primary mode at small $|n|$ (see figure 9c).

The linear spectral waves discussed so far correspond to the regime when the change of \mathcal{E}_{pri} is negligible. Eventually, though, as higher harmonics are populated and thus absorb more energy, the primary wave will be depleted. This means, in particular, that no primary wave can be truly stationary. Even an arbitrarily small perturbation will generally launch a PSW, and this PSW will eventually deplete the primary wave.

4.3. Anomalous dissipation

Since a PSW mode carries energy towards $|n| \rightarrow \infty$, eventually, a large enough $|n|$ is reached where the energy is dissipated regardless of how small the viscosity and resistivity are. Thus, a PSW exhibits an effective, or ‘anomalous’, dissipation rate γ that is independent of ν and η in the limit $\nu, \eta \rightarrow 0$. This effect is different from the anomalous transport caused by eddy–eddy collisions in turbulence (for example, see Donzis, Sreenivasan & Yeung (2005)) in that the energy transport caused by a PSW is ballistic. As a result, γ is straightforward to calculate, which is done as follows.

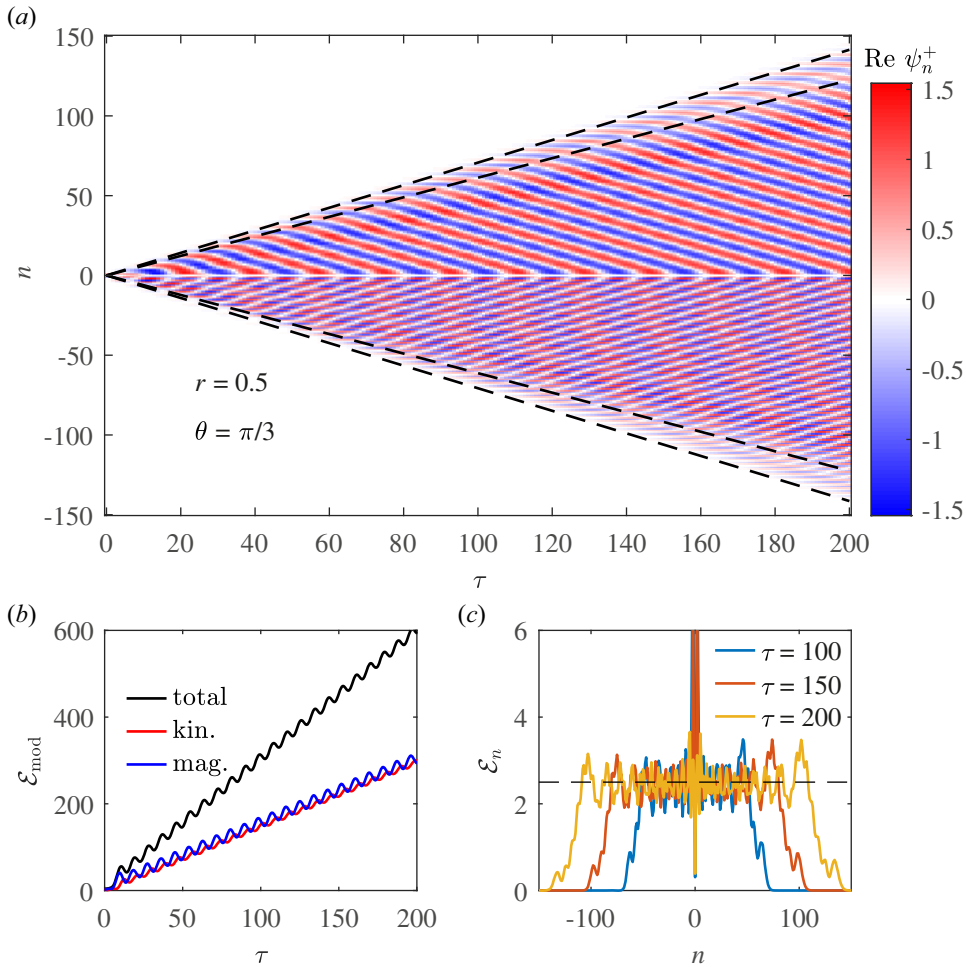


FIGURE 9. The XQLS showing global-mode PSWs for $r = 0.5$, $\theta = \pi/3$ and $\phi = \pi/4$: (a) $\text{Re } \psi_n^+ / \epsilon$ for a PSW seeded by the initial conditions (4.6) with $\xi_d^\sigma = d \exp(\sigma i \pi / 4)$ (colour bar). The dashed lines indicate the fronts propagating at (i) the maximum spectral speed $\sqrt{2}r$ and (ii) the actual group velocity of the mode. The field between these dashed lines consists of transients, which are negligible behind the second front. (b) The total normalized energy of the modulation, $\mathcal{E}_{\text{mod}} / \epsilon^2$, versus τ (black), along with its kinetic (red) and magnetic (blue) components. (c) The profiles of the spectral energy density at $\tau = 100, 150, 200$, clearly exhibiting left- and right-propagating fronts. The horizontal dashed line indicates the average spectral energy density $\overline{\mathcal{E}_n}$, where the average is taken over the PSW period and over n between the energy fronts.

As discussed in § 4.2, a global PSW at large $|n|$ has a flat mode structure, i.e. a structure with \mathcal{E}_n independent of n . This structure establishes itself as an expanding ‘shelf’ whose edges (wavefronts) propagate across the modulational spectrum to $n \rightarrow \pm\infty$ at the group velocity v_g (figure 11). Since the height of the shelf, $\overline{\mathcal{E}_n}$ (the overbar here denotes averaging over the PSW temporal period and over all n within the shelf), remains constant, this process drains energy from the primary mode linearly in time,

$$\dot{\mathcal{E}}_{\text{pri}} = -2|v_g|\overline{\mathcal{E}_n} = \text{const.}, \tag{4.9}$$

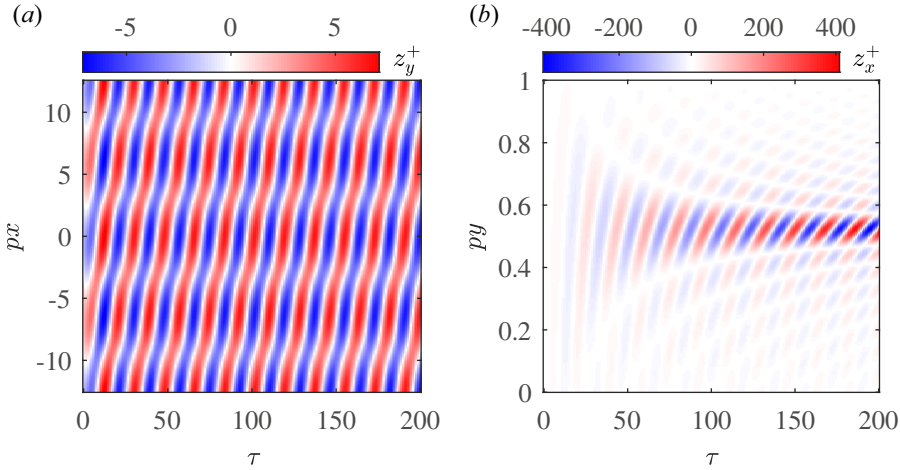


FIGURE 10. The global-mode PSW mode with $\omega > 0$, $r = 0.5$ and $\theta = \pi/3$; the same as figure 9, but in the real space as opposed to the spectral space. Specifically shown are (a) z_y^+ as a function of (τ, x) at $y = 0$; (b) z_x^+ as a function of (τ, y) at $x = 0$.

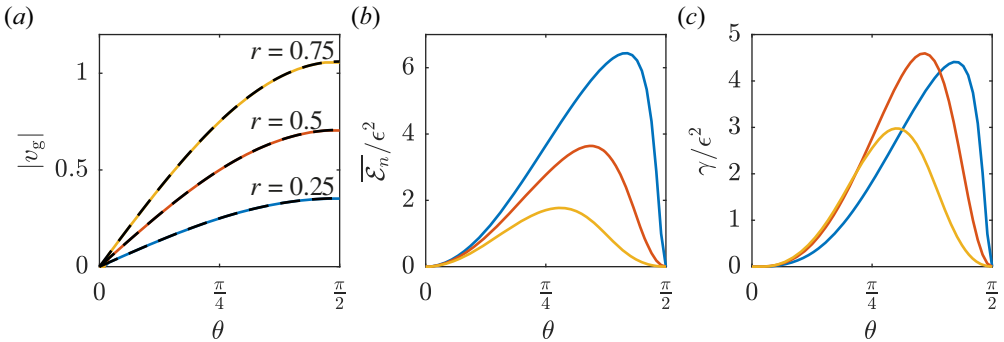


FIGURE 11. (a) The magnitude of the group velocity $|v_g|$ of the global PSW mode (i.e. the speed at which the energy front propagates along the spectrum) versus θ for various r . (b) The same for the average spectral energy density $\overline{\mathcal{E}}_n/\epsilon^2$. (c) The same for the resulting average drain rate γ/ϵ^2 , where γ is defined in (4.10). The initial conditions used throughout these figures are given by (4.6), with $\xi_1^\sigma = -\xi_{-1}^\sigma = \exp(\sigma i\pi/2)$.

where we consider the dynamics average over the PSW temporal period. Hence,

$$\gamma \doteq -\frac{\dot{\mathcal{E}}_{\text{pri}}}{\mathcal{E}_{\text{pri}}} = 2|v_g| \frac{\overline{\mathcal{E}}_n}{\mathcal{E}_{\text{pri}}} \sim \omega_0^\pm \epsilon^2. \tag{4.10}$$

(The rate relative to the physical time t , as opposed to τ , is \mathcal{A} times this γ .)

Let us again assume the initial conditions (4.6) and $\phi = \pi/4$. Through XQLS, we find that the global PSW-mode amplitude is maximized when $|\arg(\xi_{\pm 1}^\sigma/\xi_{\pm 1}^{-\sigma})| = |\arg(\xi_{\pm 1}^\sigma/\xi_{\mp 1}^\sigma)| = \pi$, irrespective of θ . (Any particular choice of ξ_n^σ that satisfies this condition affects only phases of the modulational dynamics and does not impact averaged quantities that determine γ .) This corresponds to the case when all modulational-seed energy is in the magnetic field; i.e. $\mathcal{E}_b = \mathcal{E}$ and $\mathcal{E}_v = 0$. Figure 11 shows the corresponding anomalous dissipation rate normalized to the seed energy, along with its determining

factors – the system-dependent PSW group velocity v_g and the average spectral energy density $\overline{\mathcal{E}}_n$, which is determined by the initial conditions. It can be seen that, for the MI unstable VDPMs ($\theta < \pi/4$), spectral waves are relatively slow and have a small amplitude. The transition to modulational stability occurs at $|v_g| \sim \Gamma_{4MT}$, where Γ_{4MT} is the MI growth rate predicted by 4MT. This condition can be understood as a threshold beyond which (i.e. at $|v_g| \gtrsim \Gamma$) PSWs provide a sufficiently fast escape route for the energy injected at small $|n|$, such that the positive feedback loops (see (2.34)) supporting MIs can no longer be sustained. In the context of \mathcal{PT} symmetry (§ 2.2.2), the spectral group velocity can be understood as the effective coupling between the links in the oscillator chain, connecting the energy injection from the primary mode at small n to the energy sink at $n \rightarrow \infty$. As $|v_g|$ increases with θ , the system transitions from broken to unbroken \mathcal{PT} symmetry.

Also, notice the following. If modulations at multiple qs are present, they launch independent cascades along $k = q + np$ and thus the drain on the shared primary mode will be additive. This regime is illustrated by figure 1(d–f), which show the modulational dynamics for a BDPM ($\theta = \pi/3$) seeded with noise. The rather nondescript modulational dynamics seen in figure 1(d,e) can be understood as the superposition of the many structures like that in figure 10 for various q . Also, the linear-in-time depletion of the primary mode seen in figure 1(f) can be understood as the sum of the PSW-driven energy fluxes along the constituent modulational channels.

5. Unified closure

As discussed in § 3.1, naive QMTs assume the perfectly reflecting boundary conditions (3.1) for spectral waves, thus precluding PSWs and ignoring potential dissipation at large $|n|$. One can expect that, instead of (3.1), it would be more accurate to adopt the following closure in anticipation of spectral waves:

$$\psi_{N+1}^\sigma = e^{iK^\sigma} \psi_N^\sigma \tag{5.1}$$

(and similarly for $\psi_{-(N+1)}^\sigma$). The value of K^σ is found, for given ω , from (4.3a,b),

$$e^{iK^\sigma} = \exp(-i\sigma\theta)[i\Omega^\sigma + \sqrt{1 - (\Omega^\sigma)^2}], \tag{5.2}$$

where $\Omega^\sigma \doteq \omega/\omega_0^\sigma$, and we restrict our attention to the range $|\text{Re } \Omega| \leq 1$ to avoid discontinuities, a choice which is consistent with the range of observed solutions. The sign of the square root is chosen to enforce outward propagation at $\text{Im } \omega = 0$, which also enforces that unstable solutions exponentially decay in the direction of propagation $|\exp(iK^\sigma)| < 1$.⁷ (Conversely, damped solutions grow in the direction of propagation.) As seen from figure 12, the resulting closure

$$\psi_{N+1}^\sigma = \exp(-i\sigma\theta)[i\Omega^\sigma + \sqrt{1 - (\Omega^\sigma)^2}]\psi_N^\sigma \tag{5.3}$$

leads to reasonably accurate results already $N = 2$, both for MIs and PSWs. In particular, note that $\text{Im } \omega$ is substantially suppressed relative to the predictions of QMTs, as the PSW closure captures effective dissipation to higher harmonics.⁸

Because the closure becomes exact only in the limit $N \rightarrow \infty$, it also yields spurious solutions (grey curves in figure 12) at finite N . One can understand this from the

⁷A different choice of signs would also yield formally valid solutions, but would not have the properties that correspond to PSWs of physical interest.

⁸The Landau-fluid closure (Hammett & Perkins 1990; Hammett *et al.* 1993) similarly captures effective dissipation to higher moments not included in a reduced description of an otherwise conservative theory.

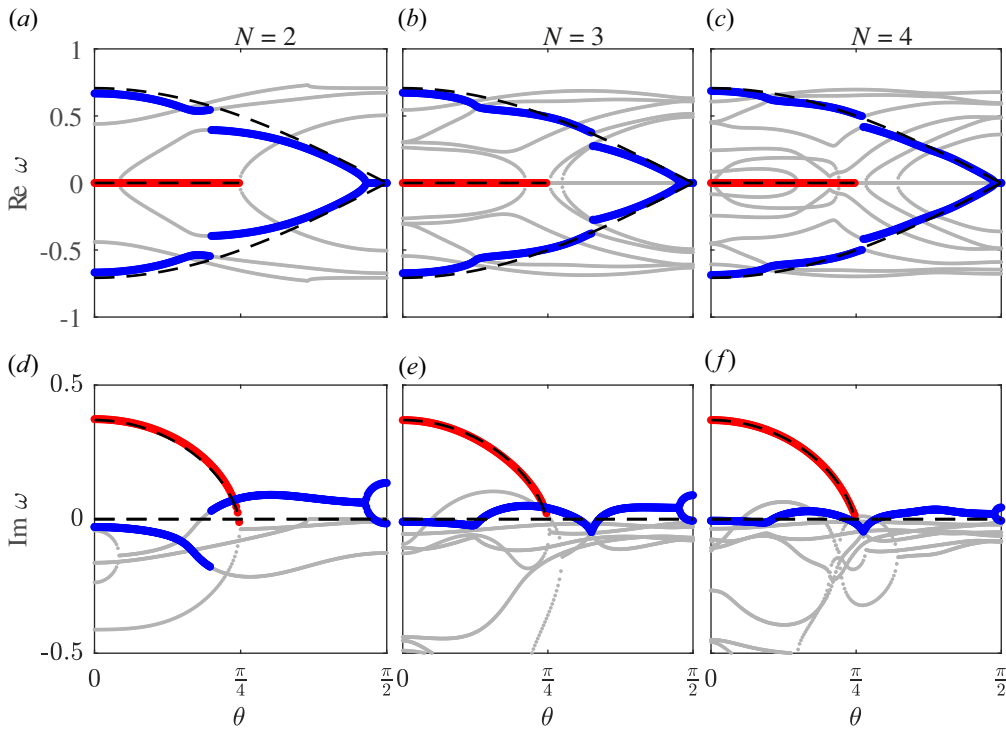


FIGURE 12. The θ -dependence of the global-mode frequencies derived from truncated models with the closure (5.3) for various N : (a–c) $\text{Re } \omega$ and (d–f) $\text{Im } \omega$. Here (a,d) $N = 2$; (b,e) $N = 3$; (c,f) $N = 4$. The red and blue curves indicate the branches that are the best match to the, respectively, unstable and stable solutions obtained through XQLS (black dashed lines). The grey curves show the remaining spurious solutions due to finite N . Note that MIs exist only for $\theta \in (0, \pi/4)$, while PSWs exist in the entire range $\theta \in (0, \pi/2)$.

analogy with the Case–van Kampen modes mentioned in § 4.2. These solutions become increasingly stable, and thus less of an issue, as N increases. Also note that the closure adequately describes true MIs. This is explained by the fact that ψ_n^σ at large $|n|$ are exponentially small and do not matter for unstable modes anyway.

6. Quasilinear approximation beyond ideal MHD

As discussed in the previous sections, the existence of PSWs undermines the standard quasilinear approximation in application to ideal incompressible MHD. Given the ubiquity of quasilinear modelling in the literature, it may seem concerning that the quasilinear approximation can fail so spectacularly. Interestingly, though, the quasilinear approximation is somewhat more robust beyond the ideal-MHD limit, both due to conservative corrections and dissipation.

Let us discuss the former first. Without attempting to describe any particular physical system, let us consider the following modified version of (2.3):

$$\partial_t \mathbf{z}^\pm = -(\mathbf{z}^\mp \cdot \nabla) \mathbf{z}^\pm - \nabla P + \hat{\chi} \mathbf{z}^\pm, \quad \hat{\chi} \doteq \lambda \partial_x \nabla^2, \tag{6.1}$$

where λ is a constant parameter. The last term is intended as a simple *ad hoc* correction that, while causing deviation from ideal MHD, leaves the primary-mode evolution unaffected and preserves MHD’s key invariants, specifically, the energy and cross-helicity

(Appendix B). Perhaps notably, this term introduces rotational asymmetry in the (x, y) plane. Similar terms can appear due to a background magnetic field or differential rotation (Heinonen *et al.* 2023).

Taking $\phi = \pi/4$ for simplicity, one arrives at the following corresponding modification of the linear (2.23):

$$\sqrt{2}(\partial_\tau + i\delta_n)\psi_n^\pm = e^{\mp i\theta}\alpha_n^-\psi_{n-1}^\pm + e^{\pm i\theta}\beta_n^-\psi_{n-1}^\mp + e^{\pm i\theta}\alpha_n^+\psi_{n+1}^\pm + e^{\mp i\theta}\beta_n^+\psi_{n+1}^\mp, \quad (6.2)$$

where $\delta_n^\pm \doteq \Lambda r(r^2 + n^2)$, $\Lambda \doteq \lambda/\mathcal{A}p^3$ and $\alpha_n^\pm, \beta_n^\pm$ are as in (2.24). In the large- $|n|$ limit, one has $\alpha_n^\pm \sim 1$, $\beta_n^\pm \rightarrow 0$, $\delta_n \sim \Lambda n^2$, so one obtains the following scaling:

$$|\psi_{n+1}^\pm| \sim \frac{|\psi_n^\pm|}{\Lambda n^2}. \quad (6.3)$$

This shows that the harmonic magnitude $|\psi_n|$ decreases rapidly (superexponentially) with $|n|$, and thus low-order truncations may be justified. Note that although the opposite scaling, $|\psi_{n-1}^\pm| \sim |\psi_n^\pm|/\Lambda n^2$ is also formally possible, such modes cannot be excited, as is the case with inward propagating PSWs. Figure 13(a) shows that, indeed, the agreement between analytical QL growth rates and XQLT improves as the parameter Λ increases. The agreement becomes nearly perfect for $\Lambda \gtrsim 0.5$. Figure 13(b) shows that the same effect can be achieved if one introduces sufficiently strong viscosity. In this case, one also has a modified (2.23) with the exact form of (6.2), but with $\hat{\chi} \doteq \nu_+ \nabla^2$ such that $\delta_n^\pm \doteq \mu(r^2 + n^2)$, where $\mu \doteq \nu_+/\mathcal{A}p^2$ (with $\nu_- = 0$ for simplicity). Again, the agreement becomes nearly exact for $\mu \gtrsim 0.5$.

More generally, note that any other linear operator $\hat{\chi}$ can be encapsulated as some δ_n . The left-hand side of (6.2) therefore determines the linear response of the system, while the right-hand side corresponds to nonlinear (modulational) dynamics, and such a decomposition into linear and nonlinear can be done for any generic system. If the linear waves of the system are dispersive, i.e. $\hat{\chi}$ is a differential operator of the second or higher order, then δ_n grows with $|n|$. Then, unless the coefficients on the right-hand side of (6.2) also grow proportionally, the amplitudes $|\psi_n^\pm|$ decrease with $|n|$ exponentially or superexponentially and PSW are not possible.

7. Summary

In this paper, we explore structure formation in 2-D MHD turbulence as a MI of turbulent fluctuations. We focus on the early stages of structure formation and consider simple backgrounds that allow for a tractable model of the MI while retaining the full chain of modulational harmonics. This approach allows for a systematic examination of the importance of high-order correlations that are typically ignored in mean-field theories.

We find that, when the primary structure truly experiences a MI, this MI can be described well with typical truncated models that neglect high-order correlations. However, already in adjacent regimes, such truncated models can fail spectacularly and produce false positives for instability. To study this process in detail, we propose an XQLT that treats the primary structure as fixed but includes the entire spectrum of modulational harmonics (as opposed to just the low-order harmonics, as usual). From XQLT, also corroborated by DNS, we find that the difference between said regimes is due to a fundamental difference in the structures of the modulational spectra. For unstable modes, the spectrum is exponentially localized at low harmonic numbers, so truncated models are justified. But this localization does not always occur. At other parameters, modulational modes turn into constant-amplitude waves propagating down the spectrum, unimpeded

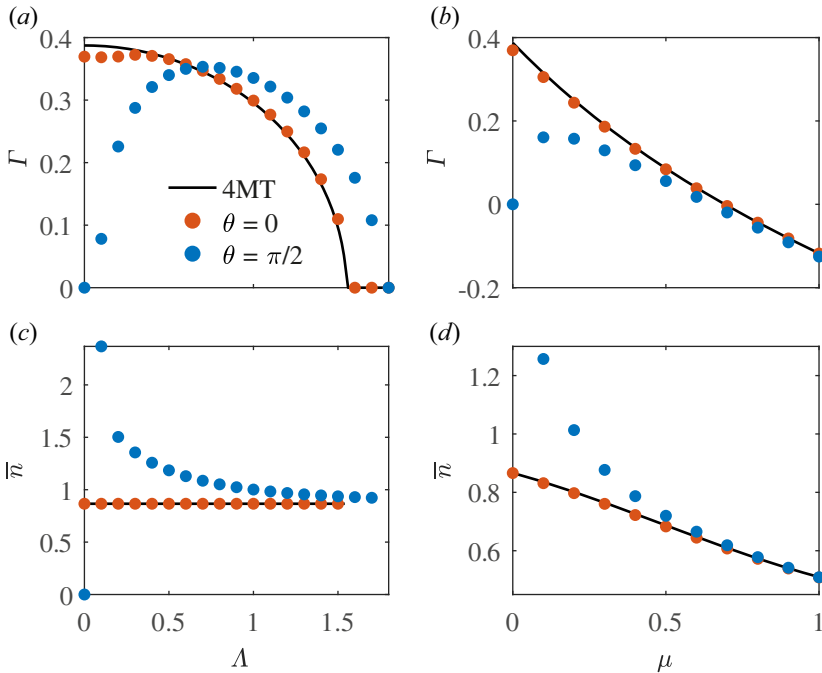


FIGURE 13. The growth rate Γ , at $\nu_- = 0$, versus (a) $\Lambda \doteq \lambda/\mathcal{A}p^3$ and (b) $\mu \doteq \nu_+/\mathcal{A}p^2$. The corresponding ‘centre of energy’ of the unstable eigenmode, $\bar{n} \doteq \sqrt{\sum_n \mathcal{E}_n n^2 / \mathcal{E}}$, is shown in (c,d), respectively. In all figures, the colour markers indicate the results obtained through XQLS, while the black solid curves indicate solutions obtained from the 4MT truncation of (6.2). The results are presented for the representative cases $\theta = 0$ and $\theta = \pi/2$, both at $r = 0.5$ and $\phi = \pi/4$.

until dissipative scales. These spectral waves are self-maintained as global modes with real frequencies and cause ballistic energy transport along the spectrum, breaking the feedback loops that could otherwise sustain MI.

The ballistic transport by PSWs drains energy from the primary structure at a constant rate until the primary structure is depleted. Because global PSWs exist at almost all parameters, this means that almost any primary structure in ideal incompressible MHD will eventually be depleted. This means, in particular, that sustainability of MHD structures is not entirely limited to the issue of exponentially growing linear instabilities, as PSWs must also be taken into consideration. To describe them within a reduced model, we propose a closure that successfully captures both the PSWs and MIs for the assumed primary structure.

Finally, we find that departures from ideal MHD constrains the form of modulational eigenmodes, in turn suppressing the amplitude and impact of high harmonics. This allows us to end on an informed yet optimistic note regarding the applicability of the quasilinear approximation for structure formation in dispersive forms of MHD. That said, it is an important conclusion of our work that, unless deviations from ideal incompressible MHD are substantial, changing the turbulence parameters even slightly can utterly destroy the applicability of an otherwise workable reduced model. An understanding of the complex modulational dynamics supported by (nearly) incompressible MHD provides important

context in the interpretation of existing simple closures and potentially opens the path to building more reliable alternatives.

Acknowledgements

S.J. thanks M. Nastac and J. Parker for helpful comments.

Editor A. Schekochihin thanks the referees for their advice in evaluating this article.

Funding

This research was supported by the U.S. Department of Energy through contract no. DE-AC02-09CH11466.

Declaration of interests

The authors report no conflict of interest.

Appendix A. Quasilinear time scale

The quasilinear approximation holds when the quasilinear MI growth rate exceeds the rate at which energy escapes to higher harmonics. In the main text, we take the latter to be the group velocity of the PSW global mode. However, one might object that the properties of PSWs are well defined only at large n , while the departure from quasilinear occurs at the modest $n = 2$. It may be instructive then to develop an alternative argument that would not assume large n . Here, we propose such an argument by considering the initial-value problem.

For simplicity, let us assume the initial conditions such that only $\psi_0(\tau = 0)$ is non-zero, with all other $\psi_{n \neq 0}(\tau = 0)$ are zero. We also adopt $(\phi, \theta) = (\pi/4, 0)$ and $(\phi, \theta) = (\pi/4, \pi/2)$ as representative cases for VDPMs and BDPMs, respectively. For these parameters, (2.28) can be further reduced due to the parity of the initial conditions. Also, the coupling matrices G_n^σ become particularly simple,

$$G_n^\sigma = \begin{cases} \frac{1}{\sqrt{2}} \begin{pmatrix} \alpha_n^\sigma & \beta_n^\sigma \\ \beta_n^\sigma & \alpha_n^\sigma \end{pmatrix}, & \theta = 0, \\ \frac{i\sigma}{\sqrt{2}} \begin{pmatrix} -\alpha_n^\sigma & \beta_n^\sigma \\ -\beta_n^\sigma & \alpha_n^\sigma \end{pmatrix}, & \theta = \frac{\pi}{2}. \end{cases} \tag{A1}$$

For the case $\theta = 0$, we assume $\psi_0^+ = \psi_0^-$ at $\tau = 0$. Then, $\dot{\psi}_n^+(\tau = 0) = \dot{\psi}_n^-(\tau = 0)$ as well, and thus $\psi_n^+ = \psi_n^-$ at all times, i.e. $\mathbf{b} \equiv 0$. We will refer to this case as \mathbf{v} -only initial conditions (VIC). The corresponding dynamics can be described by a single function $\psi_n \doteq \psi_n^+ = \psi_n^-$, which satisfies the equation

$$\dot{\psi}_n = \frac{\alpha_n^- + \beta_n^-}{\sqrt{2}} \psi_{n-1} + \frac{\alpha_n^+ + \beta_n^+}{\sqrt{2}} \psi_{n+1}. \tag{A2}$$

For the case $\theta = \pi/2$, we assume $\psi_0^+ = -\psi_0^-$ at $\tau = 0$. Similarly to the VIC case, this implies that $\mathbf{v} \equiv 0$. We will refer to this case as \mathbf{b} -only initial conditions (BIC). The corresponding dynamics can be described by a single function $\psi_n \doteq -i^n \psi_n^+ = (-i)^n \psi_n^-$,

which satisfies the equation

$$\dot{\psi}_n = \frac{\alpha_n^- - (-1)^n \beta_n^-}{\sqrt{2}} \psi_{n-1} + \frac{\alpha_n^+ - (-1)^n \beta_n^+}{\sqrt{2}} \psi_{n+1}. \tag{A3}$$

To estimate the nonlinear time scale τ_{NL} on which ψ_2 might become comparable to ψ_0 , let us consider (A2) and (A3) for $n = 2$ at early times, when ψ_3 remains negligible,

$$\ddot{\psi}_2 = \begin{cases} \frac{\alpha_2^- + \beta_2^-}{\sqrt{2}} \left(\frac{\alpha_1^- + \beta_1^-}{\sqrt{2}} \psi_0 + \frac{\alpha_1^+ + \beta_1^+}{\sqrt{2}} \psi_2 \right) & \text{for VIC,} \\ \frac{\alpha_2^- - \beta_2^-}{\sqrt{2}} \left(\frac{\alpha_1^- + \beta_1^-}{\sqrt{2}} \psi_0 + \frac{\alpha_1^+ + \beta_1^+}{\sqrt{2}} \psi_2 \right) & \text{for BIC.} \end{cases} \tag{A4}$$

Initially, $|\psi_0| \gg |\psi_2|$, so the second term in the brackets can be neglected in both cases and the nonlinear time scale can be readily estimated,

$$\tau_{NL}^{-2} = \frac{1}{2} \times \begin{cases} (\alpha_2^- + \beta_2^-)(\alpha_1^- + \beta_1^-) & \text{for VIC,} \\ (\alpha_2^- - \beta_2^-)(\alpha_1^- + \beta_1^-) & \text{for BIC.} \end{cases} \tag{A5}$$

In contrast, the quasilinear time scale τ_{QL} , which follows from the 4MT equations (3.4), is identical in both cases,

$$\tau_{QL}^{-2} = \alpha_0^- (\alpha_1^- + \beta_1^-). \tag{A6}$$

The ratio of time scales is then

$$\left(\frac{\tau_{QL}}{\tau_{NL}} \right)^2 = \begin{cases} \frac{2\sqrt{r^2 + 4}}{r + 4} & \text{for VIC,} \\ \frac{2r\sqrt{r^2 + 4}}{r + 4} & \text{for BIC.} \end{cases} \tag{A7}$$

For the range of interest ($|r| < 1$), this always yields

$$\frac{\tau_{QL}}{\tau_{NL,BIC}} < 1 < \frac{\tau_{QL}}{\tau_{NL,VIC}}. \tag{A8}$$

(For example, at $r = 0.5$, one has $\tau_{QL}/\tau_{NL,VIC} \approx 0.5$, and $\tau_{QL}/\tau_{NL,BIC} \approx 1.5$.) Thus, quasilinear is sufficient for VIC but not for BIC, in agreement with our numerical results.

Appendix B. Properties of (6.1)

The operator introduced in (6.1) conserves energy (here it is normalized to the constant mass density),

$$E \doteq \frac{1}{4} \int dx (|z^+|^2 + |z^-|^2), \tag{B1}$$

and cross-helicity,

$$H_C \doteq \frac{1}{4} \int dx (|z^+|^2 - |z^-|^2). \tag{B2}$$

These can be expressed in terms of the Elsasser energies

$$E^\pm \doteq \int dx |z^\pm|^2 / 4, \tag{B3}$$

as

$$E = E^+ + E^-, \quad H_C = E^+ - E^-. \quad (\text{B4a,b})$$

Equation (6.1) yields

$$\begin{aligned} \frac{dE^\pm}{dt} &= \frac{1}{4} \int d\mathbf{x} \partial_t |z^\pm|^2 \\ &= \frac{1}{2} \int d\mathbf{x} z^\pm \cdot \partial_t z^\pm \\ &= \frac{\lambda}{2} \int d\mathbf{x} z^\pm \cdot \partial_x \nabla^2 z^\pm \\ &= \frac{\lambda}{2} \int d\mathbf{x} z_l^\pm \partial_x \partial_m^2 z_l^\pm \\ &= -\frac{\lambda}{2} \int d\mathbf{x} (\partial_m z_l^\pm) (\partial_x \partial_m z_l^\pm) \\ &= -\frac{\lambda}{4} \int d\mathbf{x} \partial_x (\partial_m z_l^\pm \partial_m z_l^\pm) \\ &= 0. \end{aligned} \quad (\text{B5})$$

Thus,

$$\frac{dE}{dt} = \frac{dE^+}{dt} + \frac{dE^-}{dt} = 0, \quad (\text{B6})$$

$$\frac{dH_C}{dt} = \frac{dE^+}{dt} - \frac{dE^-}{dt} = 0, \quad (\text{B7})$$

meaning that (6.1) conserves both E and H_C .

REFERENCES

- ADKINS, T. & SCHEKOCHIHIN, A.A. 2018 A solvable model of Vlasov-kinetic plasma turbulence in Fourier–Hermite phase space. *J. Plasma Phys.* **84** (1), 905840107.
- BENDER, C.M. 2005 Introduction to \mathcal{PT} -symmetric quantum theory. *Contemp. Phys.* **46**, 277.
- BENDER, C.M., DOREY, P.E., DUNNING, C., FRING, A., HOOK, D.W., JONES, H.F., KUZHEL, S., LÉVAI, G. & TATEO, R. 2019 *PT Symmetry*. World Scientific.
- BERESNYAK, A. 2019 MHD turbulence. *Living Rev. Comput. Astrophys.* **5** (1), 2.
- BISKAMP, D. 2003 *Magnetohydrodynamic Turbulence*. Cambridge University Press.
- BISKAMP, D. & SCHWARZ, E. 2001 On two-dimensional magnetohydrodynamic turbulence. *Phys. Plasmas* **8** (7), 3282–3292.
- BISKAMP, D., SCHWARZ, E. & DRAKE, J.F. 1996 Two-dimensional electron magnetohydrodynamic turbulence. *Phys. Rev. Lett.* **76** (8), 1264.
- BLACKMAN, E.G. & FIELD, G.B. 2002 New dynamical mean-field dynamo theory and closure approach. *Phys. Rev. Lett.* **89**, 265007.
- BOLDYREV, S. & LOUREIRO, N. F. 2018 Calculations in the theory of tearing instability. *J. Phys.: Conf. Ser.* **1100** (1), 012003.
- BRANDENBURG, A. 2018 Advances in mean-field dynamo theory and applications to astrophysical turbulence. *J. Plasma Phys.* **84** (4), 735840404.
- BRANDENBURG, A., SOKOLOFF, D. & SUBRAMANIAN, K. 2012 Current status of turbulent dynamo theory: from large-scale to small-scale dynamos. *Space Sci. Rev.* **169**, 123–157.

- BRANDENBURG, A. & SUBRAMANIAN, K. 2005a Astrophysical magnetic fields and nonlinear dynamo theory. *Phys. Rep.* **417** (1), 1–209.
- BRANDENBURG, A. & SUBRAMANIAN, K. 2005b Minimal tau approximation and simulations of the alpha effect. *Astron. Astrophys.* **439** (3), 835–843.
- DODIN, I.Y. 2022 Quasilinear theory for inhomogeneous plasma. *J. Plasma Phys.* **88**, 905880407.
- DONZIS, D.A., SREENIVASAN, K.R. & YEUNG, P.K. 2005 Scalar dissipation rate and dissipative anomaly in isotropic turbulence. *J. Fluid Mech.* **532**, 199–216.
- ELSASSER, W.M. 1950 The hydromagnetic equations. *Phys. Rev.* **79** (1), 183.
- FRIEDBERG, J.P. 1987 *Ideal Magnetohydrodynamics*. Plenum Press.
- GALTIER, S., NAZARENKO, S.V., NEWELL, A.C. & POUQUET, A. 2000 A weak turbulence theory for incompressible magnetohydrodynamics. *J. Plasma Phys.* **63** (5), 447–488.
- GIORGIO, E.D., SERVIDIO, S. & VELTRI, P. 2017 Coherent structure formation through nonlinear interactions in 2D magnetohydrodynamic turbulence. *Sci. Rep.* **7**, 13849.
- GOPALAKRISHNAN, K. & SINGH, N.K. 2023 Mean-field dynamo due to spatio-temporal fluctuations of the turbulent kinetic energy. *J. Fluid Mech.* **973**, A29.
- GRUZINOV, A.V. & DIAMOND, P.H. 1994 Self-consistent theory of mean-field electrodynamics. *Phys. Rev. Lett.* **72** (11), 1651.
- HAMMETT, G.W., BEER, M.A., DORLAND, W., COWLEY, S.C. & SMITH, S.A. 1993 Developments in the gyrofluid approach to tokamak turbulence simulations. *Plasma Phys. Control. Fusion* **35**, 973.
- HAMMETT, G. W. & PERKINS, F. W. 1990 Fluid moment models for Landau damping with application to the ion-temperature-gradient instability. *Phys. Rev. Lett.* **64**, 3019–3022.
- HEINONEN, R.A., DIAMOND, P.H., KATZ, M.F.D. & RONIMO, G.E. 2023 Generation of momentum transport in weakly turbulent β -plane magnetohydrodynamics. *Phys. Rev. E* **107**, 025202.
- HUSSAIN, A.K.M.F. 1986 Coherent structures and turbulence. *J. Fluid Mech.* **173**, 303–356.
- KANEKAR, A., SCHEKOCIHIHIN, A.A., DORLAND, W. & LOUREIRO, N.F. 2015 Fluctuation-dissipation relations for a plasma-kinetic Langevin equation. *J. Plasma Phys.* **81** (1), 305810104.
- KÄPYLÄ, P.J., KORPI, M.J., OSSENDRIJVER, M. & STIX, M. 2006 Magnetoconvection and dynamo coefficients - III. α -effect and magnetic pumping in the rapid rotation regime. *Astron. Astrophys.* **455** (2), 401–412.
- KARIMABADI, H., ROYTERSHEYN, V., WAN, M., MATTHAEUS, W.H., DAUGHTON, W., WU, P., SHAY, M., LORING, B., BOROVSKY, J., LEONARDIS, E., *et al.* 2013 Coherent structures, intermittent turbulence, and dissipation in high-temperature plasmas. *Phys. Plasmas* **20** (1), 012303.
- KRAICHNAN, R.H. 1977 Eulerian and Lagrangian renormalization in turbulence theory. *J. Fluid Mech.* **83** (2), 349–374.
- KRASHENNIKOV, S.I., D'IPPOLITO, D.A. & MYRA, J.R. 2008 Recent theoretical progress in understanding coherent structures in edge and SOL turbulence. *J. Plasma Phys.* **74** (5), 679–717.
- KRAUSE, F. & RÄDLER, K.H. 1980 *Mean-field Magnetohydrodynamics and Dynamo Theory*. Pergamon Press.
- LINGAM, M. & BHATTACHARJEE, A. 2016 Hall current effects in mean-field dynamo theory. *Astrophys. J.* **829** (1), 51.
- MASADA, Y. & SANO, T. 2014 Mean-field modeling of an α^2 dynamo coupled with direct numerical simulations of rigidly rotating convection. *Astrophys. J. Lett.* **794** (1), L6.
- MOFFATT, H.K. 1978 *Field Generation in Electrically Conducting Fluids*. Cambridge University Press.
- NASTAC, M.L., EWART, R.J., SENGUPTA, W., SCHEKOCIHIHIN, A.A., BARNES, M. & DORLAND, W.D. 2023 Phase-space entropy cascade and irreversibility of stochastic heating in nearly collisionless plasma turbulence. [arXiv:2310.18211](https://arxiv.org/abs/2310.18211).
- NAZARENKO, S. 2007 2D enslaving of MHD turbulence. *New J. Phys.* **9** (8), 307.
- NICKLAUS, B. & STIX, M. 1988 Corrections to first order smoothing in mean-field electrodynamics. *Geophys. Astrophys. Fluid Dyn.* **43** (2), 149–166.
- PARKER, J.T. 2016 Gyrokinetic simulations of fusion plasmas using a spectral velocity space representation. [arXiv:1603.04727](https://arxiv.org/abs/1603.04727).
- PIPIN, V.V. & PROCTOR, M.R.E. 2008 Closure tests for mean field magnetohydrodynamics using a self-consistent reduced model. *Mon. Not. R. Astron. Soc.* **388** (1), 367–374.
- POUQUET, A. 1978 On two-dimensional magnetohydrodynamic turbulence. *J. Fluid Mech.* **88** (1), 1–16.

- POUQUET, A., FRISCH, U. & LÉORAT, J. 1976 Strong MHD helical turbulence and the nonlinear dynamo effect. *J. Fluid Mech.* **77** (2), 321–354.
- RÄDLER, K.H. 1982 On dynamo action in the high-conductivity limit. *Geophys. Astrophys. Fluid Dyn.* **20** (3–4), 191–211.
- RÄDLER, K.H. 2007 *Mean-Field Dynamo Theory: Early Ideas and Today's Problems*, pp. 55–72. Springer.
- RINCON, F. 2019 Dynamo theories. *J. Plasma Phys.* **85** (4), 205850401.
- RINCON, F., CALIFANO, F., SCHEKOCHIHIN, A.A. & VALENTINI, F. 2016 Turbulent dynamo in a collisionless plasma. *Proc. Natl Acad. Sci. USA* **113** (15), 3950–3953.
- SCHEKOCHIHIN, A.A. 2022 MHD turbulence: a biased review. *J. Plasma Phys.* **88** (5), 155880501.
- SCHRINNER, M., RÄDLER, K.-H., SCHMITT, D., RHEINHARDT, M. & CHRISTENSEN, U. 2005 Mean-field view on rotating magnetoconvection and a geodynamo model. *Astron. Nachr.* **326** (3–4), 245–249.
- SMOLYAKOV, A.I., DIAMOND, P.H. & MALKOV, M. 2000 Coherent structure phenomena in drift wave–zonal flow turbulence. *Phys. Rev. Lett.* **84**, 491–494.
- SQUIRE, J. & BHATTACHARJEE, A. 2015 Electromotive force due to magnetohydrodynamic fluctuations in sheared rotating turbulence. *Phys. Rev. E* **92**, 053101.
- STIX, T.H. 1992 *Waves in Plasmas*. AIP.
- TOBIAS, S.M. 2021 The turbulent dynamo. *J. Fluid Mech.* **912**, P1.
- TSIOLIS, V., ZHOU, Y. & DODIN, I.Y. 2020 Structure formation in turbulence as an instability of effective quantum plasma. *Phys. Lett. A* **384**, 126377.
- ZAKHAROV, V.E. & OSTROVSKY, L.A. 2009 Modulation instability: the beginning. *Physica D* **238**, 540.
- ZELDOVICH, Y.B. 1957 The magnetic field in the two-dimensional motion of a conducting turbulent fluid. *Sov. Phys. JETP* **4**, 460–462.
- ZHOU, H. & BLACKMAN, E.G. 2021 On the shear-current effect: toward understanding why theories and simulations have mutually and separately conflicted. *Mon. Not. R. Astron. Soc.* **507** (4), 5732–5746.
- ZHU, H. & DODIN, I.Y. 2021 Wave-kinetic approach to zonal-flow dynamics: recent advances. *Phys. Plasmas* **28**, 032303.